

STELLAR EXPLOSIONS BY MAGNETIC TOWERS

DMITRI A. UZDENSKY¹ & ANDREW I. MACFADYEN²

(Dated: May 20, 2019)
Draft version May 20, 2019

ABSTRACT

We propose a magnetic mechanism for the collimated explosion of massive stars relevant for long-duration gamma-ray bursts (GRBs), X-ray Flashes (XRFs) and asymmetric core collapse supernovae. In particular, we apply Lynden-Bell's magnetic tower scenario to the interior of a massive rotating star after the core has collapsed to form a collapsar with a black hole accretion disk or a millisecond magnetar as the central engine. The key element of the model is that the pressure of the toroidal magnetic field, continuously generated by differential rotation of the central engine, drives a rapid expansion which becomes vertically collimated after lateral force balance with the surrounding gas pressure is reached. The collimation naturally occurs because hoop stress concentrates magnetic field toward the rotation axis and inhibits lateral expansion without affecting vertical expansion. This leads to the growth of a self-collimated magnetic structure which Lynden-Bell termed a *magnetic tower*. When embedded in a massive star, the supersonic expansion of the tower drives a strong bow shock behind which an over-pressured cocoon of shocked stellar material forms, as observed in hydrodynamical simulations of collapsar jets. The cocoon confines the tower by supplying collimating pressure support and provides stabilization against disruption due to magnetohydrodynamical instabilities. Because the tower consists of closed field lines starting and ending on the central engine, mixing of baryons from the cocoon into the tower is suppressed. Baryon loading due to magneto-centrifugal winds from the central engine may also be suppressed because of the expected field line geometry. The channel cleared by the growing tower is thus plausibly free of baryons and allows the escape of magnetic energy from the central engine through the star. While propagating down the stellar density gradient, the expansion of the tower accelerates and becomes relativistic. At some point during the expansion fast collisionless reconnection becomes possible. The resulting dissipation of magnetic energy into accelerated particles may be responsible for GRB prompt emission.

Subject headings: accretion, accretion disks — magnetic fields — MHD — gamma rays: bursts — supernovae: general — stars: magnetic fields

1. INTRODUCTION

Long duration gamma-ray bursts (GRBs) are asymmetric explosions (Harrison et al. 1999; Stanek et al. 1999) associated with the death of massive stars (Matheson et al. 2003; Hjorth et al. 2003; Stanek et al. 2003). Spectroscopic observations of the afterglow of GRB030329 revealed a bright underlying Type Ibc supernova, SN2003dh (Matheson et al. 2003; Stanek et al. 2003), which bore close resemblance to SN1998bw, the first supernova associated with a GRB, the faint nearby (40 Mpc) GRB980425 (Galama et al. 1998). Two other convincing spectroscopic identifications of supernovae associated with XRF020903 (Soderberg 2005) and GRB031203 (Malesani et al. 2004) have been reported in addition to about ten photometric detections (Zeh, Klose & Hartmann 2004; Soderberg et al. 2006). It is now firmly established observationally that some, perhaps all, of the long duration GRBs are associated with Type Ibc supernovae (though the converse is not the case). Evidence for strong asymmetry in GRB ejecta is derived from the afterglow light curves which exhibit, after several days, an achromatic transition in the power law decay of brightness as a function of time, indicating that the explosion was beamed into jets with opening angle of ~ 10 degrees. Taken together, these observations show that some supernova explosions involve strongly asymmetric relativistic outflow. Massive stars are thus observed to be capable, in some cases, of producing strongly

collimated energetic outflows when they die.

Such asymmetry is naturally expected in models where the progenitor star is rapidly rotating when it collapses and subsequently explodes. Stellar rotation breaks spherical symmetry and provides the rotation axis as a preferred direction along which jet-like outflow can develop. Observations of massive stars do indicate rapid surface rotation velocities (Fukuda 1982), though the distribution of angular momentum in the cores of evolved stars when they undergo core collapse is uncertain (Spruit 2002; Heger, Woosley & Spruit 2005; Maeder & Meynet 2005). However, low metallicity is expected to be beneficial for maintaining angular momentum in the core until collapse (MacFadyen & Woosley 1999, Hirschi, Meynet, & Maeder 2005). Current stellar evolution models do, in some cases, predict rapid rotation in collapsing cores of massive single stars (Heger, Woosley & Spruit 2005), perhaps aided by global mixing (Woosley & Heger 2005; Yoon & Langer 2005). It is also expected that membership in a tight binary system will endow some massive stars with rapid rotation in their cores when they die (Fryer & Heger 2005, Petrovic 2005) though the angular momentum imparted to the core depends on detailed transport processes (Petrovic et al. 2005).

A theoretical model for long duration GRBs based on rapid stellar rotation is known as the *collapsar* (Woosley 1993; Paczynski 1998; MacFadyen & Woosley 1999; MacFadyen, Woosley & Heger 2001) in which the core of a massive rotating star collapses to form a black hole. Numerical simulations have shown that, in rapidly rotating stars, an accretion disk rapidly forms around the young black hole (MacFadyen &

¹ Princeton University, Department of Astrophysical Sciences, Peyton Hall, Princeton, NJ 08544; uzdensky@astro.princeton.edu.

² Institute for Advanced Study, Princeton, NJ 08540; aim@ias.edu.

Woosley 1999). Because of angular velocity gradients in the disk, the magneto-rotational instability (MRI) is expected to develop, providing angular momentum transport and dissipation of gravitational energy. At the temperatures and densities ($T \sim 4 \times 10^{10}$ K, $\rho \sim 10^{10}$ g cm $^{-3}$) present in collapsar disks, neutrino emission can cool the accreting gas with a range of efficiency. The collapsing outer stellar core is therefore able to accrete at rates of $\sim 0.1 M_{\odot} s^{-1}$ for times $\gtrsim 10$ s providing sufficient energy for sufficiently long times to power long GRBs.

Magnetohydrodynamical (MHD) simulations have demonstrated the development of MRI in collapsar disks (Proga et al. 2003). Magnetic fields approaching equipartition values in excess of 10 15 G are then expected to develop as the disk forms. In addition, field strengths approaching 10 15 G may develop during collapse as seed poloidal field winds up into toroidal field. Similar processes, resulting in similar field strengths, are also believed to be taking place in core-collapse supernovae explosions (Akiyama et al. 2003).

Because gas along the rotation axis of the star does not experience a centrifugal barrier, it falls into the black hole unimpeded, thus lowering the density above the hole to $\rho \lesssim 10^6$ gm cm $^{-3}$. Similarly to its role in Type II supernovae explosions (Goodman et al. 1987), neutrino annihilation may be important in the low density funnel above the black hole, heating the stellar gas and causing it to expand along the rotation axis of the star. Under favorable conditions this hot gas can form a collimated relativistic outflow which is capable of escaping the stellar surface and forming a fireball. MacFadyen & Woosley (1999) explored this possibility but noted that magnetic processes are an alternate mechanism capable of extracting energy from the system. In fact, the suggestion that strongly magnetized jets play an active role in GRB explosions (perhaps via a version of the Blandford-Znajek mechanism) has been invoked by several authors (e.g., Thompson 1994; Meszaros & Rees 1997; Lee et al. 2000; Vlahakis & Königl 2001; van Putten & Ostriker 2001; Drenkhahn & Spruit 2002; Lyutikov & Blandford 2003; van Putten & Levinson 2003; Proga et al. 2003; Lyutikov 2004, 2006; Lei et al. 2005; Proga & Zhang 2006).

In this paper, motivated by the above considerations, we consider a possible magnetic mechanism for driving a low-baryon-load, Poynting-flux dominated jet through a massive collapsing star. In order to understand the structure of magnetic jets in massive stars we investigate a simple analytic model that may help guide interpretation of detailed MHD simulations.

Our paper is organized as follows. In § 2 we describe the key physical ideas that underlie our model. The main idea is that we apply the *magnetic tower* mechanism, developed previously by Lynden-Bell (1996) for active galactic nucleus (AGN) jets, to the collapsar environment. We first give a qualitative description of Lynden-Bell's original model (in an accretion disk geometry) and derive some basic scalings resulting from it (§ 2.1). In the rest of § 2, we present our picture of a magnetic tower growing rapidly inside a star and driving a strong shock through it. Thus, in § 2.2, we describe our modifications to the original magnetic tower model; the most important of these is that the external pressure confining the tower is no longer arbitrary but is determined self-consistently by the hot gas *cocoon* surrounding the tower and by the strong shock driven into the star. In § 2.3 we derive simple scalings for the tower parameters and then, in § 2.4, we use these scalings to make some quantitative estimates. In § 3

we make the next step and present mathematical formalism of our model. Our analysis is characterized by representing the time evolution of the tower by a sequence of force-free magnetostatic equilibria, obtained by solving the Grad-Shafranov equation with additional constraints and boundary conditions that, in general, change with time. We then present, as examples, several particular analytical solutions (in § 4). After that, in § 5, we discuss the implications of our model for gamma-ray bursts and outline some important open issues that we feel need to be addressed in future research. In particular, in § 5.1 we argue that, as the tower expands in a stratified star, the unperturbed stellar density at the top of the tower drops and the expansion process accelerates. At a certain point, the tower growth will then have to make a transition to the relativistic regime, which is not covered by our theory. Nevertheless, we speculate that the tower will remain collimated, with an opening angle of a few degrees. In § 5.2 we discuss the tower structure and the distribution of magnetic energy inside the tower. In § 5.3 we discuss the issue of baryon contamination originating from the disk as a result of neutrino ablation and magneto-centrifugal winds. Next, in § 5.4, we discuss various MHD instabilities that may be excited in the system and the effect they may have on the evolution of the magnetic tower. In § 5.5, we discuss the question of whether the tower can be disrupted through reconnection while it is still deep inside the star and argue against this possibility. In § 5.6 we outline numerical simulations which may be performed to explore the model. We present our conclusions in § 6.

Finally, note that for definiteness we develop our model in the context of the original collapsar scenario, where the central engine is an accretion disk around a black hole. The energy source in this case is accretion energy. However, we believe that a similar magnetic tower mechanism may also work when the central engine is a young millisecond magnetar born inside a collapsing star. The typical values of the magnetic field strength, the rotation rate, and the size of the system are similar in the two cases. The overall electro-magnetic luminosities should therefore also be comparable (e.g., Usov 1992; Thompson 1994). The energy source for the explosion in the magnetar case is the rotational energy of the neutron star and the magnetic field acts as an agent that extracts this energy. The basic mechanism is essentially similar to that proposed by Ostriker & Gunn (1971) for powering supernovae light-curves by the spin-down magnetic luminosity of a rapidly-rotating pulsar (with the magnetic field scaled up by three orders of magnitude and the timescale scaled down by six). In fact, several models invoking rapidly-rotating magnetars as central engines for GRBs have been proposed (e.g., Usov 1992; Thompson 1994; Yi & Blackman 1998; Thompson et al. 2004; Lyutikov 2006). However, these models usually don't discuss the geometry (e.g., collimation) of the outflow. In addition, they typically consider an isolated magnetar (without a surrounding stellar envelope). The collimating influence of the dense stellar material is thereby neglected. We believe that a rapidly-rotating magnetar will make an even better central engine when considered within the collapsar framework. A simplified physical model representing this scenario is the *pulsar-in-a-cavity* problem. By analyzing this problem, we can show that, even though the magnetar itself rotates uniformly, a strong differential rotation is effectively established on the field lines extending beyond the light cylinder. As a result, toroidal magnetic flux is constantly injected into the cavity and eventually toroidal magnetic field becomes dominant over both the poloidal magnetic field and the electric field in

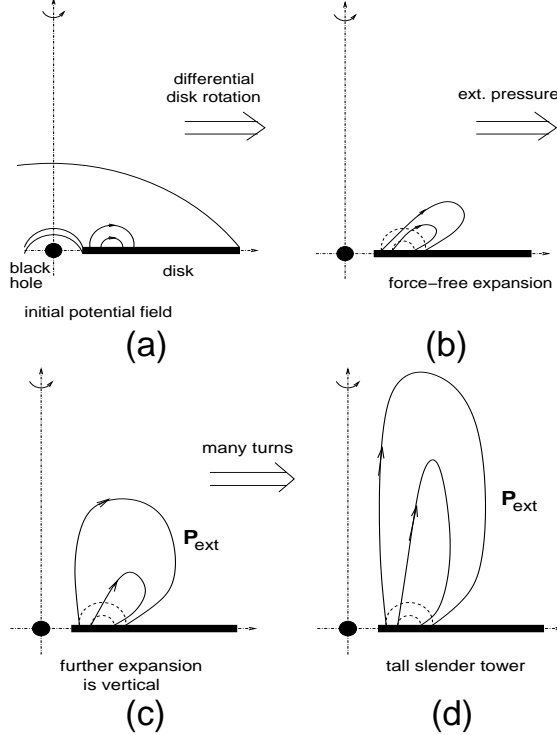


FIG. 1.— Development of a magnetic tower in Lynden-Bell's (1996) model.

the magnetosphere. Any subsequent expansion of the cavity is then going to be mostly vertical because of the collimating hoop stress, just as in Lynden-Bell's (1996) model. Eventually, a magnetic tower forms. In our opinion, this pulsar-in-a-cavity problem, viewed as a paradigm for a millisecond-magnetar-driven GRB explosion mechanism, is very important by itself. Therefore we believe it deserves a separate study and we intend to pursue it in an upcoming paper.

2. MAGNETIC TOWER: BASIC PHYSICAL PICTURE

2.1. Lynden-Bell's Original Magnetic Tower Model

As a specific mathematical vehicle to illustrate our ideas, we choose the *magnetic tower* introduced by Lynden-Bell (1996, 2003). A magnetic tower is an axisymmetric magnetic configuration that arises when a system of nested closed flux surfaces, anchored in a differentially-rotating disk, is twisted and, as a result, inflates, but when this inflation is controlled by a surrounding external pressure. The basic physical mechanism of this process can be described as follows (see Fig. 1).

Consider a thin conducting disk with some vertical magnetic flux frozen into it. Let us assume that initially the magnetic field is potential and has a fully-closed dipole-like topology (see Fig. 1a), with the two footpoints of each field line located at different radii on the disk. Now let us assume that the disk rotates non-uniformly, which is certainly the case for a Keplerian disk. Then, each field line Ψ is twisted at a rate $\Delta\Omega(\Psi)$ equal to the difference in angular velocities of the two footpoints of this line. Correspondingly, toroidal magnetic flux is generated from the poloidal flux. The pressure of this toroidal field pushes the flux surfaces outward, against the poloidal field tension. It is assumed that during the initial stages of this process the gas pressure, as well as the gravitational and inertial forces, are negligibly small in the disk

magnetosphere, so the magnetic field is force-free. Then the expansion is uncollimated, typically along the direction making a 60° angle with respect to the rotation axis (Fig. 1b). However, as was shown by Lynden-Bell (1996), if there is some, no matter how small, external gas pressure that surrounds the expanding disk magnetosphere, then at some point the sideways expansion is stopped. This is because the magnetic field strength at the outermost portions of inflating field lines decreases rapidly during the inflation process; then, once $B^2/8\pi$ drops to the level of the external gas pressure, any further horizontal expansion ceases. However, as again was shown by Lynden-Bell (1996), the story doesn't end here; unable to expand sideways, the twisted magnetosphere expands in the vertical direction (Fig. 1c), eventually forming a slender cylindrical column that Lynden-Bell termed a *magnetic tower* (see Fig. 1d). If the external pressure outside of the tower is kept constant and uniform, then the top of the tower rises at a constant speed. Plasma inertia never plays any role in this process; the entire evolution is viewed as a sequence of magnetostatic equilibria, with the field being force-free inside the tower and with pressure balance between the external gas outside of the tower and the magnetic field inside.

Note that the assumption that both ends of a field line connect to the disk itself is actually not essential. An alternative configuration, with a very similar overall behavior, is that of a rotating conducting rotating central star (a proto-neutron star in the collapsar context) or even a rotating black hole. In the conducting star case, the differential star-disk rotation leads to the same field-line inflation and opening process in the force-free regime (e.g., Lovelace et al. 1995; Uzdensky et al. 2002), followed by the tower stage when the external pressure becomes important. A very similar process takes place when a conducting disk is connected magnetically to a rapidly-rotating black hole: even though a black hole cannot be considered a good conductor, general-relativistic frame-dragging ensures that a closed-field configuration that extends far enough on the disk cannot stay in equilibrium and therefore has to inflate and open up (Uzdensky 2005; see also McKinney 2005).

Since the first analytical solution proposed by Lynden-Bell (1996), the magnetic tower concept is becoming more and more accepted by the astrophysical community. For example, the formation and evolution of magnetic towers have been studied in numerical simulations (Li et al. 2001; Kato et al. 2004) and even in real laboratory experiments (Hsu & Bellan 2002; Lebedev et al. 2005).

In order to get accurate quantitative results, one needs to consider a specific solution of the governing MHD equations with some particular boundary conditions. However, to get a basic physical feeling of how the magnetic tower grows, it is instructive to derive some simple order-of-magnitude estimates and scaling relationships. In Lynden-Bell's (1996) model, the main input parameters that determine the solution are the total poloidal magnetic flux Ψ_0 (per unit toroidal angle) in the tower, the characteristic differential rotation rate $\Delta\Omega$, and the external pressure P_{ext} . In the rest of this section we investigate how the main parameters that characterize the tower, namely, its radius, the typical magnetic field, and the growth velocity, scale with these three input parameters.

First, we estimate the radius of the tower, R_0 , and the characteristic poloidal magnetic field strength, B_{pol} . They are ob-

viously related via

$$B_{\text{pol}} \sim B_0 \equiv \frac{\Psi_0}{R_0^2}. \quad (1)$$

As we mentioned earlier, the radius adjusts so that the magnetic pressure inside the tower equals the external gas pressure. From the force-free balance inside the tower we expect the toroidal magnetic field to be roughly the same as the poloidal field: $B_\phi \sim B_{\text{pol}} \sim B_0$. The total magnetic field strength at the outer edge of the tower is thus also of the order of B_0 . Then, from the condition of pressure balance across the tower's side wall we get

$$B_0 \sim \sqrt{8\pi P_{\text{ext}}}. \quad (2)$$

By combining this with equation (1), we get

$$R_0 \sim \left(\frac{\Psi_0^2}{8\pi P_{\text{ext}}} \right)^{\frac{1}{4}}. \quad (3)$$

Next, let us estimate the rate of growth of the tower. To do this, we use the fact that the toroidal magnetic flux is continuously generated out of the poloidal flux by the differential rotation. Every time a given flux tube with poloidal flux $\Delta\Psi$ is twisted by one full turn, the amount of toroidal flux carried by the tube is increased by $\Delta\Psi$. Therefore, after $N = \Delta\Omega t/(2\pi)$ turns the total toroidal flux χ in the tower becomes

$$\chi = 2\pi\Psi_0 N = \Psi_0 \Delta\Omega t. \quad (4)$$

Assuming that this toroidal flux fills the tower uniformly and that the tower is a cylinder with radius R_0 and height Z_{top} , we see that the characteristic toroidal field has to be of the order of

$$B_\phi \sim \frac{\chi}{R_0 Z_{\text{top}}} = \frac{\Psi_0}{R_0 Z_{\text{top}}} \Delta\Omega t = B_0 \frac{R_0}{Z_{\text{top}}} \Delta\Omega t. \quad (5)$$

However, as we stated earlier, the typical toroidal field in the tower is of the order B_0 ; therefore, the height of the tower has to increase steadily as

$$Z_{\text{top}}(t) \sim R_0 \Delta\Omega t. \quad (6)$$

In other words, the tower grows at the speed comparable to the typical differential rotation velocity $R_0 \Delta\Omega$. If the external pressure does not change, the radius of the tower, determined by equation (3), stays constant during its growth; therefore, after many turns ($\Delta\Omega t \gg 1$), the height Z_{top} becomes much larger than the radius, i.e., the tower becomes slender.

2.2. Magnetic Tower Driving a Shock through a Star

As we mentioned briefly in the Introduction, we believe that there are several good reasons that make the magnetic tower mechanism an attractive model for the formation and propagation of a magnetically-dominated jet through a star within the collapsar model for GRBs (and perhaps core-collapse supernovae as well). To reiterate, a configuration where all the field lines close back onto the central engine (e.g., an accretion disk or a magnetar) is very natural for a field created by a turbulent dynamo (with zero net flux). In addition, diffusion of particles across the field is suppressed and thus baryon contamination of the tower from the stellar envelope is inhibited. This is in contrast with the models that invoke the Blandford-Znajek mechanism operating directly along open field lines inside the star. Even if a light, ultra-relativistic outflow is

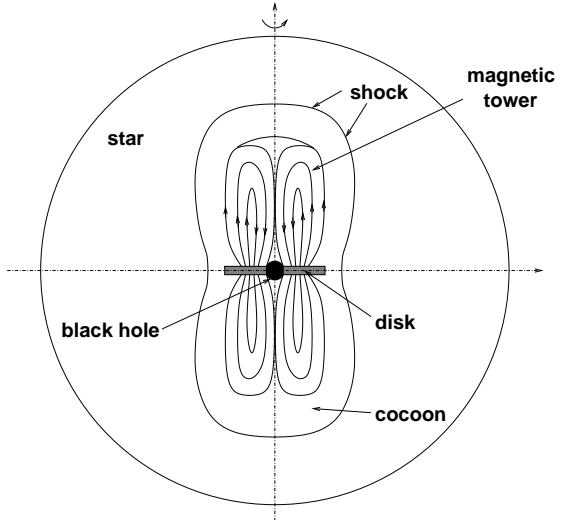


FIG. 2.— The main components of our model. A magnetic tower grows rapidly and drives a strong shock through the star. The shocked stellar gas behind the shock forms a hot cocoon whose high pressure confines the tower.

launched along such field lines, it will first have to push all the baryonic matter, already present on these field lines, ahead of itself; therefore, the resulting ejecta in these models will not be baryon-free. On the other hand, the closed-field geometry, characteristic of the magnetic tower model, at least eliminates this problem. The only way baryons can get into the tower is via a wind blowing from the disk or the neutron star. An assessment of baryon contamination due to a wind is an important issue that we will discuss in § 5.3.

In order to apply the magnetic tower model to the collapsar scenario, we first have to make a few modifications to Lynden-Bell's original picture. Specifically, we extend his model by taking into account the high-pressure cocoon that surrounds and confines the tower. In our model, the magnetic tower grows very rapidly and thus acts as a piston driving a shock ahead of it. The shocked stellar gas above the tower has very high pressure; it therefore squirts sideways and forms backflows that fill the cocoon around the tower as described for AGN jets by Begelman, Blandford and Rees (1984) (see Fig. 2). Therefore, the external pressure that confines the tower is no longer an arbitrary parameter, in contrast with Lynden-Bell's model. Instead, it is determined by the jump conditions across the shock surrounding the cocoon across the contact discontinuity between the cocoon and the tower. Since the speed at which the magnetic tower plows through the star is much higher than the sound speed in the unperturbed stellar material, the external unperturbed pressure of the star is irrelevant; it should thus be excluded from our list of the three main input parameters used for our simple, order-of-magnitude estimates. Instead, the expansion of the cocoon is controlled by the ram pressure related to the gas *inertia*; therefore, we replace the external pressure by the unperturbed stellar density ρ_0 in the list of basic dimensional parameters (along with Ψ_0 and $\Delta\Omega$) that determine the relevant physical scales in our problem. This change represents an important difference between our model and Lynden-Bell's.

The actual situation is complicated further by the two-dimensional character of the problem. Indeed, since the sound speed inside the cocoon is very high, comparable to the speed at which the tower grows, gas pressure tends to be partially

equalized throughout the cocoon. This expectation is supported by the hydrodynamic numerical simulations³ of the collapsar model by MacFadyen et al. (2001) and Zhang et al. (2003), which show that, typically, the variation of the cocoon pressure along its length is relatively weak, just a factor of 5 or 10. This is very moderate compared to the corresponding variations of the unperturbed stellar density and pressure, which both vary by many orders of magnitude along the vertical extent of the cocoon. As a result, the gas pressure is very high everywhere in the cocoon so the cocoon also drives a sideways shock into the star. Thus, the boundary between the tower and the cocoon is a contact discontinuity, whereas the boundary between the cocoon and the rest of the star is a two-dimensional strong shock of some complicated shape.

We see that, in principle, the problem calls for a consideration of the entire *two-dimensional* shock-cocoon-tower structure. For simplicity, however, we shall represent the cocoon by only two components: the hot spot right above the tower (with some uniform pressure P_{top}) and the cylindrical shell surrounding the tower on the sides (with a different uniform pressure P_{side}). Thus, we shall parameterize the pressure non-uniformity in the cocoon by the ratio $\eta = P_{\text{side}}/P_{\text{top}}$. In accordance with this 2-component cocoon structure, we shall represent the strong shock between the cocoon and the star also by two components: a plane shock that propagates purely vertically above the tower and a slower cylindrical shock that propagates sideways. An important difference between these two shocks is that, whereas the upward shock is driven exclusively by the vertical growth of the magnetic tower, the sideways shock is driven mostly by the pressure of the hot gas that flows into the side part of the cocoon from the top hot spot; the horizontal expansion of the tower may also play a role in driving the sideways shock, but probably to a lesser extent.

Let us now discuss what determines η . We use simple energetics considerations for a rough estimate. The energy flux that is required to drive the sideways shock is of order $P_{\text{side}}V_{s,\text{side}}$, where $V_{s,\text{side}}$ is the speed of the sideways shock; it is, in turn, proportional to the sound speed, $V_{s,\text{side}} \sim (P_{\text{side}}/\rho_{0,\text{side}})^{1/2}$. In our simple 2-component model, the area of the sideways shock is larger than the area of the vertical shock by a factor $\kappa \equiv Z_{\text{top}}R_{\text{cocoon}}/R_0^2 \gg 1$. Thus, in order for the power necessary to maintain the sideways shock not to exceed the available thermal power generated by the vertical growth of the tower, one must satisfy

$$\eta \leq \kappa^{-2/3} \left(\frac{\rho_{0,\text{side}}}{\rho_{0,\text{top}}} \right)^{1/3}. \quad (7)$$

Thus, we see that, as the tower grows (and κ increases) with time, $\eta = P_{\text{side}}/P_{\text{top}}$ tends to decrease, but, on the other hand, this decrease is partially weakened by the density non-uniformity, i.e., by the large ratio $\rho_{0,\text{side}}/\rho_{0,\text{top}}$. We also see that the sideways shock propagates noticeably slower than the vertical shock. This is due to a combination of two factors: a smaller (by a factor of η) pressure driving the sideways shock and a higher background density of the stellar gas into which the sideways shock is propagating. As a result, the cocoon is moderately elongated in the vertical direction, with an aspect

³ Note that, even though the simulations by MacFadyen et al. (2001) and Zhang et al. (2003) do not include magnetic fields, they probably still give a reasonably good qualitative representation of the cocoon behavior even in our magnetic tower scenario, since the cocoon itself remains unmagnetized.

ratio of

$$\frac{Z_{\text{cocoon}}}{R_{\text{cocoon}}} \sim \frac{V_{s,\text{top}}}{V_{s,\text{side}}} \sim \eta^{-1/2} \sqrt{\frac{\rho_{0,\text{side}}}{\rho_{0,\text{top}}}} \sim \left(\kappa \frac{\rho_{0,\text{side}}}{\rho_{0,\text{top}}} \right)^{1/3}. \quad (8)$$

These estimates, of course, are only as good as the underlying two-component cocoon structure assumed here. In a realistic situation, where the tower is growing in a strongly stratified medium, the radii of both the tower and the cocoon are not going to be constant in the vertical direction. In that situation, one cannot represent the tower and the cocoon by straight cylinders; instead, one has to describe their shapes by some increasing functions $R_0(z)$ and $R_{\text{cocoon}}(z)$.

2.3. Simple Estimates

Let us now show how the basic properties of the growing magnetic tower are expressed in terms of the three parameters Ψ , $\Delta\Omega$, and ρ_0 . For simplicity, in this and the next subsections, we ignore the non-uniformity of the gas pressure in the cocoon, i.e., we set $\eta = 1$. We will reinstate this non-uniformity and study the dependence of the tower growth parameters on η in our more rigorous analysis of §§ 3–4.

For simplicity we shall use shock jump conditions corresponding to a one-dimensional problem. Since the gas pressure of the unperturbed stellar material upstream of the shock is neglected, the shock is strong. Assuming a gas with an adiabatic index 5/3, the shock velocity with respect to the unperturbed gas is $V_s = 4/3 V_{\text{top}}$, whereas the pressure in the post-shock region (i.e., in the cocoon) can be expressed in terms of the velocity of the piston $V_p \equiv V_{\text{top}}$ and the upstream gas density ρ_0 as (see, e.g., Kulsrud 2005)

$$P_{\text{top}} = \frac{3}{4} \rho_0 V_s^2 = \frac{4}{3} \rho_0 V_{\text{top}}^2. \quad (9)$$

By comparing this result with the condition of pressure balance $P_{\text{top}} \simeq B_0^2/8\pi$ at the contact discontinuity at the top of the tower, we immediately see that the tower grows with a velocity of order the Alfvén speed computed with the unperturbed density ρ_0 :

$$V_{\text{top}} \sim V_A \equiv \frac{B_0}{\sqrt{4\pi\rho_0}} = \frac{\Psi_0}{R_0^2 \sqrt{4\pi\rho}}. \quad (10)$$

On the other hand, as we have shown earlier, V_{top} should be of the order of the differential rotation speed $R_0\Delta\Omega$. Thus, we obtain the following estimate for the radius of the tower in terms of Ψ_0 , $\Delta\Omega$, and ρ_0 :

$$R_0 \sim \left(\frac{\Psi_0}{\Delta\Omega} \right)^{1/3} (4\pi\rho_0)^{-1/6}. \quad (11)$$

We can also relate the radius of the tower to the radius of the central accretion disk. The poloidal flux Ψ_0 can roughly be estimated as

$$\Psi_0 \sim B_d R_d^2, \quad (12)$$

where B_d is the typical magnetic field in the disk (or, rather, its dipole-like part), and R_d is the characteristic radius of the inner part of the disk — the base of the tower. Then,

$$B_0 \sim B_d \frac{R_d^2}{R_0^2}, \quad (13)$$

and

$$\frac{R_0}{R_d} \sim \left(\frac{\tilde{V}_{A,d}}{V_d} \right)^{1/3}, \quad (14)$$

where $V_d \equiv R_d \Delta\Omega$ is the characteristic differential rotation velocity in the disk (on the order of the Keplerian velocity V_K) and

$$\tilde{V}_{A,d} \equiv \frac{B_d}{\sqrt{4\pi\rho_0}} \quad (15)$$

is a convenient composite quantity that has a form of an Alfvén speed involving the disk magnetic field and the unperturbed star's plasma density; it doesn't represent a physical velocity and so can be arbitrarily high; in particular, it can be greater than the speed of light.

Notice that as the tower makes its way through the star, two of the three main parameters, Ψ_0 , and $\Delta\Omega$, remain unchanged, but the third parameter, the unperturbed stellar density ρ_0 measured at the top Z_{top} of the tower, changes. In fact, it drops rather rapidly for a typical collapsar progenitor. Correspondingly, the radius of the tower increases as the tower grows.

Also notice that, by assumption, the pressure spreads rapidly along the cocoon. Therefore, the characteristic magnetic field and hence the radius of the tower are more or less constant along the tower at any given time. This justifies the assumption that the tower is a straight cylinder. In a more general situation, when the pressure equilibration in the cocoon lags somewhat, the radius of the tower will be a function of the vertical coordinate z . However, as is seen from equation (11), R_0 scales only weakly with ρ_0 (as $\rho_0^{-1/6}$). This fact enables us to regard the constant density case as a good approximation.

2.4. Let's Do the Numbers

Now we will use the above relationships to make some quantitative estimates based on the scaling relationships obtained in the previous section; thus, unavoidably, these estimates can only provide order-of-magnitude estimates.

We assume that the core of the star has collapsed into a black hole of fiducial mass $M = 3M_{\odot}$ with a corresponding gravitational radius $R_g \equiv GM/c^2 \simeq 5\text{ km}$, and that some of the continuously infalling material has formed an accretion disk around the black hole. The pre-existing stellar magnetic field has been greatly amplified by the collapse because of flux-freezing and by the turbulent dynamo in the disk. Akiyama & Wheeler (2003) have argued that the field may reach the level set by the equipartition with the MRI-driven turbulence, as strong as 10^{16-17} G . This field is mostly toroidal, however; hence the large-scale poloidal magnetic field that we need in our model will have to be somewhat smaller. Thus, we believe it is not unreasonable for the poloidal field at the disk surface to be a more modest $B_d \sim 10^{15}\text{ G}$ (see also Proga et al. 2003).

Now, if we take fiducial disk radius of $R_d \simeq R_{\text{ISCO}}(a = 0) = 6R_g \simeq 3 \cdot 10^6\text{ cm}$, where a is the normalized Kerr parameter of the black hole, we may have an initial poloidal dipole flux per unit toroidal angle of the order of $\Psi_0 = R_d^2 B_0 \simeq 10^{28} B_{15} R_{d,6.5}^2$ in cgs units. (Note that if the black hole is spinning rapidly, then the inner disk radius is actually much closer, $R_{\text{ISCO}} \simeq R_g \simeq 5\text{ km}$.) This poloidal flux is being continuously twisted by the differential Keplerian rotation of the disk, with characteristic angular velocity $\Delta\Omega = \Omega_K(R_d) \simeq 4 \cdot 10^3 \text{ sec}^{-1} (M/3M_{\odot})^{1/2} R_{d,6.5}^{-3/2}$.

The typical background density of the stellar material into which the tower propagates is $\rho_0 = 10^6 \text{ g/cm}^3$. This corresponds to the quantity $\tilde{V}_{A,d}$ of the order of $3 \cdot 10^{11} \text{ cm/sec}$ for a 10^{15} G magnetic field. Hence, according to equation (14), the

tower radius can be estimated as

$$R_0 \sim R_d \left(\frac{\tilde{V}_{A,d}}{V_d} \right)^{\frac{1}{3}} = 3R_d \left(\frac{B_{d,15}}{R_{d,6.5} \Delta\Omega_{3.5} \sqrt{\rho_{0,6}}} \right)^{1/3}, \quad (16)$$

resulting in $R_0 \simeq 10^7 \text{ cm}$ for our fiducial parameter values.

Using this estimate for the outer radius of the tower, we can get the following expressions for all the other parameters:

$$\begin{aligned} B_0 &\equiv \frac{\Psi_0}{R_0^2} = B_d \left(\frac{R_d}{R_0} \right)^2 \\ &\simeq 0.1 B_d \left(\frac{R_{d,6.5} \Delta\Omega_{3.5}}{B_{d,15}} \right)^{2/3} \rho_{0,6}^{1/3} \simeq 10^{14} \text{ G}; \end{aligned} \quad (17)$$

$$V_{A,0} \equiv \frac{B_0}{\sqrt{4\pi\rho_0}} = 3 \cdot 10^{10} \text{ cm/sec } B_{d,15}^{1/3} R_{d,6.5}^{2/3} \Delta\Omega_{3.5}^{2/3} \rho_{0,6}^{-1/6} \quad (18)$$

Notice that our crude estimate results in $V_{\text{top}} \sim V_{A,0}$ being comparable to the speed of light c ; moreover, as we shall show in § 4, a growth velocity of $V_{\text{top}} \simeq 2.5V_{A,0}$ is actually more typical. These facts strongly suggest that a fully-relativistic treatment of the problem would be more appropriate (see § 5.1 for discussion). Such a treatment lies beyond the scope of the current paper, but we do intend to develop the relativistic magnetic tower theory in a subsequent paper.

Also, we can estimate the post-shock pressure in the hot cocoon above the tower as

$$P_{\text{top}} \simeq \frac{B_0^2}{8\pi} \simeq 4 \cdot 10^{26} \text{ erg cm}^{-3} B_{0,14}^2. \quad (19)$$

where $B_{0,14} \equiv B_0/(10^{14}\text{ G})$. At such very high energy densities the radiation pressure most likely dominates over the gas pressure; we can therefore estimate the plasma temperature in the post-shock region as

$$T_{\text{top}} \simeq \left(\frac{3P_{\text{top}}}{a} \right)^{1/4} \simeq 2 \cdot 10^{10} \text{ K} \simeq 2 \text{ MeV}, \quad (20)$$

where $a \simeq 7.6 \cdot 10^{-15} \text{ erg cm}^{-3} \text{ K}^{-4}$. On the other hand, since we are dealing with a strong hydrodynamic shock between the cocoon and the unperturbed stellar material, the baryon density in the cocoon is simply $4\rho_0$, and so the baryon rest-mass energy density is $4\rho_0 c^2 \simeq 4 \cdot 10^{27} \text{ erg cm}^{-3} \rho_{0,6}$, and hence still exceeds the radiation/pair energy density by an order of magnitude.

The total magnetic energy contained in the tower of height Z_{top} can be estimated as

$$E_{\text{mag}} \simeq 2\pi R_0^2 Z_{\text{top}} \frac{B_0^2}{8\pi} \simeq 2 \cdot 10^{50} \text{ erg } R_{0,7}^2 Z_{\text{top},9} B_{0,14}^2, \quad (21)$$

which represents a noticeable fraction of a typical GRB energy (the factor 2 is added to take into account the fact that we actually have two towers, one above and one below the disk midplane).

3. MATHEMATICAL FORMALISM

The estimates presented in the previous section are very rough. A more rigorous mathematical model is needed to demonstrate how magnetic towers work and to obtain more accurate quantitative estimates of the tower growth parameters. We shall proceed to construct such a model. In particular, we shall develop a general analysis in this section and then use it in § 4 to illustrate our model by specific examples.

Consider a magnetic tower making its way through a star. Since the system is axisymmetric, the magnetic field can be written in cylindrical polar coordinates (R, ϕ, z) as

$$\mathbf{B}(R, z) = \mathbf{B}_{\text{pol}} + B_\phi \hat{\phi} = \frac{1}{R} [\nabla \Psi \times \hat{\phi}] + \frac{I_{\text{pol}}}{R} \hat{\phi}, \quad (22)$$

where $\Psi(R, z)$ is the poloidal magnetic flux function, $I_{\text{pol}}(R, z)$ is $(2/c)$ times the poloidal electric current, and $\hat{\phi}$ is the toroidal unit vector. If the magnetic field inside the tower is force-free, I_{pol} is constant along poloidal field lines, $I_{\text{pol}}(R, z) = I_{\text{pol}}(\Psi)$.

We shall focus on the middle part of Lynden-Bell's magnetic tower (his section II), where the poloidal magnetic field is nearly straight and vertical. For simplicity we shall assume that the outer radius of the tower, R_0 , is independent of height z . This means that, at any given moment of time t , all magnetic quantities depend only on one coordinate — the cylindrical radius R . Then, the force-free Grad-Shafranov equation — the main *partial* differential equation (PDE) that governs the field structure — reduces to a 2nd-order *ordinary* differential equation (ODE) for the function $\Psi(R)$:

$$R \partial_R \left(\frac{1}{R} \Psi_R \right) = -I_{\text{pol}} I'_{\text{pol}}(\Psi), \quad (23)$$

supplemented by two boundary conditions,

$$\Psi(R = 0) = \Psi_0 = \Psi(R = R_0). \quad (24)$$

As a side remark, we could consider a more general situation where the outer radius slowly changes with height, $R_0 = R_0(z)$. Then, instead of just one ODE, we would have a one-parameter infinite set of ODEs, one for each height z . All these equations would have the same form as equation (23); the local height z would come in indirectly through the outer boundary condition $\Psi = \Psi_0$ at $R = R_0(z)$.

Equation (23) involves a free function, the poloidal current $I_{\text{pol}}(\Psi)$. In reality, this function is not arbitrary but is determined by the differential rotation of the footpoints. By a simple geometrical consideration, the twist angle $\Delta\Phi(\Psi)$ (i.e., 2π times the number of rotations) can be written as

$$\Delta\Phi(\Psi) = I_{\text{pol}}(\Psi) \int_{\Psi} \frac{dl_{\text{pol}}}{R^2 B_{\text{pol}}} = I_{\text{pol}}(\Psi) \int_{\Psi} \frac{dz}{R^2 B_z}, \quad (25)$$

where the integration is performed along the field line and l_{pol} is the path length along the poloidal field. Assuming that most of the twist occurs in the main part of the magnetic tower, where the poloidal field is nearly vertical, we can write:

$$\Delta\Phi(\Psi) = I_{\text{pol}}(\Psi) Z_{\text{top}}(t) \left[\frac{1}{R_1(\Psi)|B_{z1}(\Psi)|} + \frac{1}{R_2(\Psi)|B_{z2}(\Psi)|} \right], \quad (26)$$

where $Z_{\text{top}}(t)$ is the total height of the tower; its time-dependence reflects the fact that the tower grows with time. Here, $R_1(\Psi)$ and $R_2(\Psi)$ are the cylindrical radii of the two segments of the flux surface Ψ , and $B_{z1}(\Psi)$ and $B_{z2}(\Psi)$ are the values of the vertical magnetic field on these segments.

On the other hand, the twist angle is determined by the disk rotation law,

$$\Delta\Phi(\Psi) = \Delta\Omega(\Psi)t. \quad (27)$$

where $\Delta\Omega(\Psi)$ is the difference between the angular velocities of the two disk footpoints of the field line Ψ . Thus, determining the twist angle really requires the knowledge of both the radial disk rotation profile, $\Omega_d(r)$, and the radial distribution of the poloidal magnetic flux on the surface of the

disk, $\Psi_d(r)$. Whereas there exists a very natural choice for the first of these two functions — the Keplerian rotation law, $\Omega_d(r) = \Omega_K(r) \sim r^{-3/2}$, the second function, i.e., $\Psi_d(r)$, is not very well known. In reality it is determined by complicated MHD processes of turbulent dynamo and turbulent magnetic flux transport, which are presently understood only poorly and definitely lie beyond the scope of this paper. Therefore, instead of pretending that we know how $\Psi_d(r)$ is really determined, we shall regard this function as essentially arbitrary. Correspondingly, instead of specifying it explicitly, we shall choose an indirect prescription dictated mostly by our mathematical convenience. In particular, we shall take $\Psi_d(r)$ to be such as to result in a convenient and simple functional form for $I_{\text{pol}}(\Psi)$. Thus, we shall use the following scheme: first, we shall pick a function $I_{\text{pol}}(\Psi)$ that will make our calculations easier; then, we shall solve the Grad-Shafranov equation for this choice of $I_{\text{pol}}(\Psi)$; and finally, we shall use equation (26) to find $\Delta\Omega(\Psi)$ and hence $\Psi_d(r)$ a posteriori. This approach is similar to what is known as the “generating-function method” in the theory of force-free equilibria (e.g., Uzdensky 2002). Even though the main logic of such a scheme is physically backwards, it makes sense to use it as long as we don't get an unreasonable functional form for $\Psi_d(r)$ in the end. At any rate, the alternative direct method, based on an explicit specification of $\Psi_d(r)$ and on a subsequent use of equation (26) to determine the corresponding $I_{\text{pol}}(\Psi)$, would be more difficult to implement and, at the same time, would also lack a good physical justification since the prescription for $\Psi_d(r)$ would necessarily be quite arbitrary.

That said, there are some important features that this function is expected to have. For example, we expect the separatrix Ψ_s to correspond to the polarity inversion line on the disk surface, i.e., a line where $B_{z,d}$ goes through zero. In general, however, the first radial derivative of $B_z(r)$ is not zero, and so generically, we expect the disk poloidal flux function to behave as $\Psi_d \simeq \Psi_s + O[(r - r_s)^2]$ near this point. Since the first radial derivative of $\Omega_K(r)$ is finite at this point, we may expect that

$$\Delta\Omega(\Psi) \sim \sqrt{|\Psi - \Psi_s|}, \quad \text{as } \Psi \rightarrow \Psi_s. \quad (28)$$

Next, we need to determine the radius R_0 of the tower. This is done by equilibrating the inside magnetic pressure to the outside cocoon gas pressure at R_0 :

$$\frac{B_\phi^2(R_0)}{8\pi} + \frac{B_z^2(R_0)}{8\pi} = P_{\text{side}}. \quad (29)$$

For simplicity we shall assume that the pressure is more or less uniform throughout the side part of the cocoon and constitutes a certain fixed fraction η of the gas pressure in the post-shock region directly above the tower: $P_{\text{side}} = \eta P_{\text{top}}$, $\eta \leq 1$. The latter, in turn, is determined from the condition of force balance across the contact discontinuity at the top of the magnetic tower. Following Lynden-Bell (1996), we ignore the complications resulting from the complex shape of this boundary and treat the tower top as a solid circular lid of radius R_0 . Then we only need to satisfy the integral force balance, which can be written as

$$P_{\text{top}} = \frac{F_z}{\pi R_0^2}, \quad (30)$$

where F_z is the total magnetic force acting on the top of the tower. It can be computed by integrating the vertical flux of momentum associated with Maxwell's stress over the tower's

cross-section:

$$F_z = 2\pi \int_0^{R_0} \left[\frac{B_\phi^2(R)}{8\pi} - \frac{B_z^2(R)}{8\pi} \right] R dR. \quad (31)$$

Using equation (22), we can rewrite this as

$$F_z = \frac{1}{4} \int_0^{R_0} \left[I_{\text{pol}}^2 - (\partial_R \Psi)^2 \right] \frac{dR}{R}. \quad (32)$$

Finally, once the pressure at the top of the tower is known, we can use equation (9) to estimate the speed at which the tower expands vertically,

$$V_{\text{top}} = \dot{Z}_{\text{top}} = \sqrt{\frac{3}{4} \frac{P_{\text{top}}}{\rho_0}}. \quad (33)$$

3.1. Formulation of the Problem in Dimensionless Variables

In the following, it will be convenient to rescale R by the tower radius R_0 , poloidal flux Ψ by the total flux in the tower Ψ_0 , and poloidal current I_{pol} by Ψ_0/R_0 . Thus we define new dimensionless variables

$$x \equiv \frac{R}{R_0}, \quad (34)$$

$$\psi \equiv \frac{\Psi}{\Psi_0}, \quad (35)$$

$$I \equiv \frac{I_{\text{pol}} R_0}{\Psi_0}. \quad (36)$$

It will also be useful to introduce a characteristic magnetic field strength

$$B_0 \equiv \frac{\Psi_0}{R_0^2}. \quad (37)$$

The Grad-Shafranov equation (23) can be written in these dimensionless variables as

$$x \partial_x \left(\frac{1}{x} \psi_x \right) = -II'(\psi). \quad (38)$$

Geometrically, the magnetic tower consists of two regions (see Fig. 3):

- 1) inner region I of descending poloidal flux: $0 \leq x \leq x_s$;
- 2) outer region II of ascending poloidal flux: $x_s \leq x \leq 1$.

The boundary between these two regions is the separatrix surface $x = x_s$. By assumption, each field line leaving the disk and rising up in region I will come back down to the disk through region II; therefore the total amount of poloidal flux in the two regions is the same. We shall need to solve the Grad-Shafranov equation (38) separately in each of these two regions and then match the solutions at the separatrix. Correspondingly, we set the boundary conditions as:

$$\psi^I(x=0) = \psi^{II}(x=1) = 1, \quad (39)$$

$$\psi^I(x=x_s) = \psi^{II}(x=x_s) = \psi_s. \quad (40)$$

Without losing generality, from now on we shall set $\psi_s = 0$.

The position of the separatrix x_s is determined from the force-balance condition across it:

$$(B_\phi^2 + B_z^2)^I = (B_\phi^2 + B_z^2)^{II} \quad (41)$$

This condition can be greatly simplified, however. Indeed, first, because $B_\phi = I_{\text{pol}}(\psi)/R$ and because the two sides of

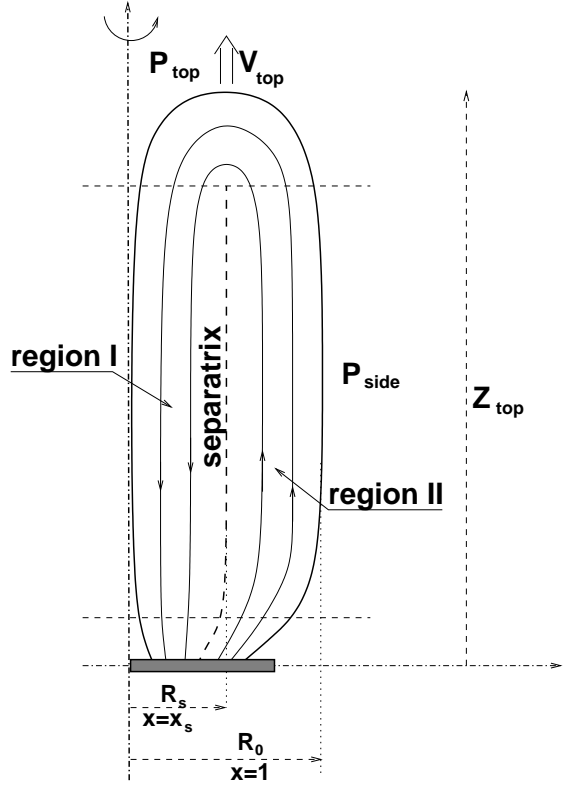


FIG. 3.— A schematic drawing of a magnetic tower.

the separatrix correspond to the same field line $\psi = \psi_s$, and hence $I^I(\psi_s) = I^{II}(\psi_s)$, we have $(B_\phi^2)^I = (B_\phi^2)^{II}$. (Moreover, we shall actually assume that $I \rightarrow \sqrt{\psi} \rightarrow 0$ near the separatrix, so B_ϕ actually goes to zero at the separatrix.) Thus, our force-balance condition becomes:

$$(B_z^2)^I = (B_z^2)^{II} \Rightarrow \psi_x^I = -\psi_x^{II} \quad \text{at } x = x_s. \quad (42)$$

The vertical force F_z is

$$F_z = \frac{1}{4} B_0^2 R_0^2 \int_0^1 [I^2(\psi) - \psi_x^2] \frac{dx}{x}, \quad (43)$$

and hence the pressure at the top of the tower is

$$P_{\text{top}} = \frac{1}{4\pi} B_0^2 \int_0^1 [I^2(\psi) - \psi_x^2] \frac{dx}{x}, \quad (44)$$

The condition (29) of pressure balance across the side wall of the tower, $x = 1$, then becomes

$$\begin{aligned} I^2(\psi = 1) + \psi_x^2(x=1) &= 8\pi \frac{P_{\text{side}}}{B_0^2} = 8\pi\eta \frac{P_{\text{top}}}{B_0^2} \\ &= 2\eta \int_0^1 [I^2(\psi) - \psi_x^2] \frac{dx}{x}, \end{aligned} \quad (45)$$

Finally, we can rewrite the expression (25) for the field-line twist angle $\Delta\Phi(\Psi)$ in our dimensionless variables as

$$\Delta\Phi(\psi) = I(\psi) \frac{V_{\text{top}}}{R_0} t \left[\frac{1}{x_1 |\psi_x(x_1)|} + \frac{1}{x_2 |\psi_x(x_2)|} \right], \quad (46)$$

where $x_1 = x_1(\psi)$ and $x_2 = x_2(\psi)$ are the radial positions of the inner and outer segments of field line ψ , respectively.

4. EXAMPLES

When dealing with any complicated physical system, it is often useful to have at hand a few analytical examples that could be used to explicitly illustrate the general characteristic behavior of the system. In our particular problem, the simplest way to obtain explicit analytical solutions is to consider the cases in which the Grad–Shafranov equation (38) becomes linear. The most general functional form of $I(\psi)$ that leads to a linear Grad–Shafranov equation is

$$I(\psi) = \sqrt{a\psi^2 + b\psi + c}. \quad (47)$$

For simplicity, we shall consider the situation where the poloidal current vanishes along the separatrix, $I(\psi = 0) = 0$, which makes $c = 0$. Other choices for c are possible and may result in interesting solutions. For now we consider $c = 0$ and thus have

$$I(\psi) = \sqrt{\psi} \sqrt{a\psi + b}. \quad (48)$$

There are several interesting special cases that we will consider in this section.

4.1. Case 1: a Configuration without a Central Line Current

First, we shall consider the case in which $I(\psi)$ behaves as $\sqrt{\psi}$ near the separatrix $\psi = 0$ and at the same time goes to zero at the rotation axis: $I(1) = 0$. Thus we choose $b = -a \equiv \mu^2 > 0$ in equation (48) and hence

$$I(\psi) = \mu \sqrt{\psi} \sqrt{1 - \psi}, \quad (49)$$

which corresponds to $-II'(\psi) = \mu^2(\psi - 1/2)$.

By substitutions $\psi = xu(x) + 1/2$, this equation is reduced to the Modified Bessel's equation $x^2u'' + xu' - u(\mu^2x^2 + 1) = 0$, and so the general solutions in the two regions can be written in terms of modified Bessel's functions as:

$$\psi_I(x) = \frac{1}{2} + a_1 x I_1(\mu x) + b_1 x K_1(\mu x), \quad (50)$$

$$\psi_{II}(x) = \frac{1}{2} + a_2 x I_1(\mu x) + b_2 x K_1(\mu x). \quad (51)$$

Here, a_1 , b_1 , a_2 , and b_2 are the arbitrary integration constants. They are determined by the boundary conditions (39)–(40) that can be cast as a linear system of four equations. Solving this system we get the explicit expressions for these coefficients in terms of the parameter μ and the position of the separatrix x_s :

$$a_1 = -\mu \frac{1 + y K_1(y)}{2y I_1(y)}, \quad (52)$$

$$b_1 = \frac{\mu}{2}, \quad (53)$$

$$a_2 = -\frac{1}{2y} \frac{y K_1(y) + \mu K_1(\mu)}{I_1(y) K_1(\mu) - K_1(y) I_1(\mu)}, \quad (54)$$

$$b_2 = \frac{1}{2y} \frac{y I_1(y) + \mu I_1(\mu)}{I_1(y) K_1(\mu) - K_1(y) I_1(\mu)}, \quad (55)$$

where we defined $y \equiv \mu x_s$ to simplify notation.

Next, the separatrix position x_s as a function of μ is determined by the separatrix force-balance condition (42) that can be written as

$$(a_1 + a_2) I_1'(y) + (b_1 + b_2) K_1'(y) = \frac{\mu}{y^2}. \quad (56)$$

Thus, we get a non-trivial transcendental algebraic equation that determines y as a function of μ . Once the solution of this

equation is found, we can use equations (55) to calculate the entire magnetic field structure. We solved equation (56) numerically using *Mathematica*. We found that the resulting dependence $y(\mu)$ is very close to linear $y = \mu/\sqrt{2}$ for small and finite values of μ . For $\mu \gg 1$ the slope of the linear dependence slightly changes and the asymptotic behavior becomes $y(\mu \rightarrow \infty) \simeq \mu - 7$. Correspondingly, the function $x_s(\mu)$ varies from $1/\sqrt{2}$ for $\mu \rightarrow 0$ to 1 for $\mu \rightarrow \infty$. [The small- μ behavior is very easy to understand: it corresponds to the situation in which the toroidal field is negligibly small, and so the horizontal force balance dictates that the magnitude of the vertical field be uniform inside the tower. Since the total upward vertical flux must be equal to the total downward flux, this means that the area of region I must be equal to that of region II; hence the separatrix between them has to be at $x_s = 2^{-1/2}$.]

Finally, we need to fix the value of μ . We do this by using the condition (29) of pressure balance between the magnetic field in the tower and gas pressure in the cocoon that surrounds and confines the tower. As discussed in § 3, this condition can be viewed as the condition that determines the tower's radius once the poloidal current I_{pol} is specified. Here we, in effect, turn this around and determine μ (which sets the overall scale for I_{pol}) in terms of the tower's radius.

The solution of course depends on the assumed value of η . For a given η , one can obtain a series of solutions for various values of μ and then find the value $\mu_0(\eta)$ for which condition (29) is satisfied. We have done this using *Mathematica* and found that the allowable range of η is limited. Namely, solutions exist only for $\eta > \eta_c \approx 0.08$, with $\mu_0(\eta)$ diverging as $(\eta - \eta_c)^{-1}$ in the limit $\eta \rightarrow \eta_c$. Both P_{top} and V_{top} also diverge and x_s approaches unity as $\eta \rightarrow \eta_c$.

We then investigated a few values of η in more detail. For $\eta = 1$ we found $\mu_0(\eta = 1) \simeq 6.70$ and $x_s(\eta = 1) \simeq 0.705$ (just a little less than $1/\sqrt{2}$). The corresponding magnetic field components as functions of x are plotted in Figure 4 (the top two panels). We see that both the vertical and toroidal field components increase towards the axis, with $B_\phi \sim x^{-1/2}$. At the separatrix (marked on the plots by the vertical dashed line), the vertical field, as expected, reverses, whereas the toroidal field goes to zero on both sides of the separatrix as $|x - x_s|^{1/2}$. The post-shock pressure above the tower is found to be $P_{\text{top}}(\eta = 1) \simeq 0.945 B_0^2$ and the vertical expansion speed of the tower, given by equation (33), is $V_{\text{top}}(\eta = 1) \simeq 3 V_{A,0}$.

It is interesting to note that, as can be seen in the top left panel of Figure 4, the vertical magnetic flux tends to be pushed out (by the toroidal field pressure) from the intermediate-radii parts of each of the two tower regions ($x \sim 0.4 - 0.5$ in region I and $x \sim 0.8$ in region II). As η decreases, this effect becomes even more pronounced, as can be seen from the bottom left panel of Figure 4 which corresponds to $\eta = 0.3$. Also, in agreement with an earlier discussion, the pressure at the top of the tower, P_{top} , expressed in units of B_0^2 , and the tower growth velocity, V_{top} , expressed in units of the Alfvén speed $V_{A,0}$, both grow rapidly as η decreases. For example, in the case $\eta = 0.3$, presented in the bottom two panels of Figure 4, we find $P_{\text{top}}(\eta = 0.3) \simeq 8.4 B_0^2$ and $V_{\text{top}}(\eta = 0.3) \simeq 8.9 V_{A,0}$.

4.2. Case 2: a Configuration with a Central Line Current

Let us now consider the case $a = 0$. Then,

$$I(\psi) = \sqrt{b\psi} \equiv \lambda \sqrt{2\psi}. \quad (57)$$

Notice that the poloidal current in this model does not van-

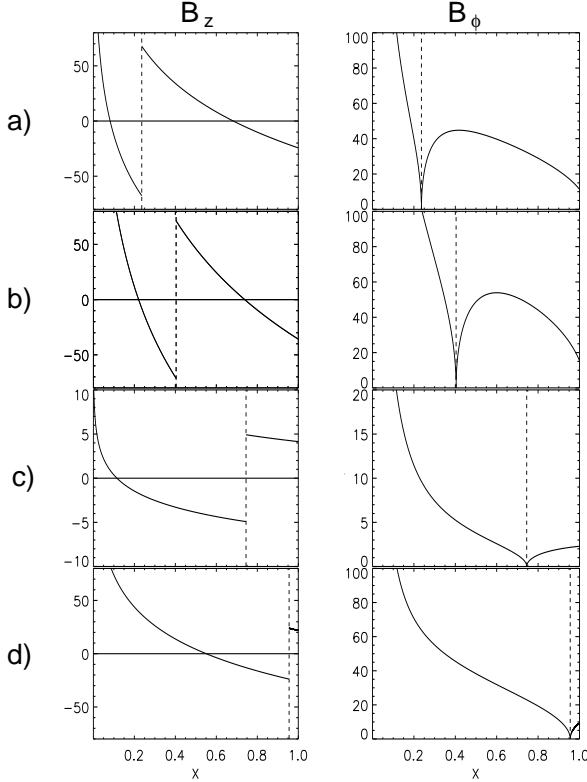


FIG. 4.— Vertical (left) and toroidal (right) magnetic field components for two solutions in Case 1, computed for $\eta = 1.0$ (top panels) and $\eta = 0.3$ (bottom panels). The vertical dashed lines on each plot shows the position x_s of the separatrix, across which the vertical field component (B_z) reverses sharply [the toroidal (B_ϕ) component is symmetric with respect to x_s].

ish at the tower's rotation axis $\psi = 1$, implying the existence of a non-zero axial line current. Such a current may represent, for example, a very narrow core jet surrounded by the magnetic tower, perhaps produced by the Blandford–Znajek (1977) mechanism acting along the field lines that thread the black hole. This line current may have important implications for the tower's growth speed and collimation, as we will discuss below.

The Grad–Shafranov equation (38) becomes:

$$x \partial_x \left(\frac{\psi_x}{x} \right) = -\lambda^2 = \text{const}, \quad (58)$$

and can be easily integrated:

$$\psi(x) = -\lambda^2 \frac{x^2}{2} \log x + C_1 \frac{x^2}{2} + C_2. \quad (59)$$

This expression represents the general solution of the 2nd-order differential equation (58). It involves two arbitrary integration constants, C_1 and C_2 , that are determined by the boundary conditions (39)–(40). The resulting final expressions for $\psi(x)$ in the two regions are:

$$\psi^I(x) = -\frac{\lambda^2}{2} x^2 \log \left(\frac{x}{x_s} \right) + 1 - \frac{x^2}{x_s^2}, \quad (60)$$

$$\psi^{II}(x) = -\frac{\lambda^2}{2} \left(x^2 \log x - \frac{1-x^2}{1-x_s^2} x_s^2 \log x_s \right) + \frac{x^2 - x_s^2}{1-x_s^2}. \quad (61)$$

Finally, the position x_s of the separatrix is obtained by substituting these solutions into the separatrix force-balance

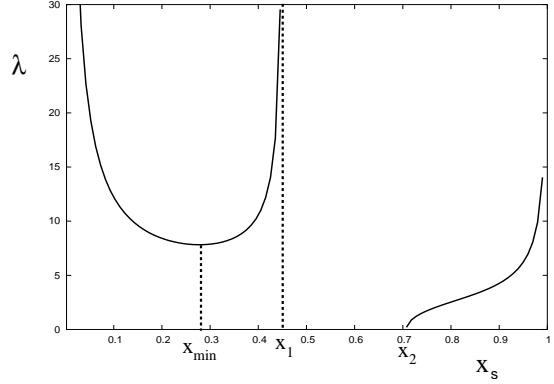


FIG. 5.— The function $\lambda(x_s)$ corresponding to equation (62) for our Case 2.

condition (42), yielding a transcendental algebraic equation for $x_s(\lambda)$. This equation can actually be resolved with respect to λ as a function of x_s , resulting in an explicit expression:

$$\lambda(x_s) = \frac{2}{x_s} \sqrt{\frac{x_s^2 - 1/2}{1 - x_s^2 + \log x_s}}. \quad (62)$$

This function is plotted in Figure 5. One can see that there are two separate allowed ranges of x_s : $0 < x_s < x_1$, and $x_2 \leq x_s < 1$, where $x_1 \approx 0.45076$, and $x_2 \equiv 1/\sqrt{2} \approx 0.707$. At $x_{\min} \approx 0.278$ the function has a minimum $\lambda(x_{\min}) \approx 7.824$. For $x_s > x_2$, the solution $\lambda(x_s)$ increases monotonically starting from $\lambda = 0$ at $x_s = x_2$ and diverges as $\lambda \sim [2/(1-x_s)]^{1/2}$ as $x_s \rightarrow 1$.

The next step in our program is to use the obtained solution to determine the vertical expansion velocity of the tower, V_{top} . To do this, we first need to compute the integrated magnetic stress on the tower's top, given by equation (43). Notice, however, that in this model, as in any model with a non-zero line current along the axis, the toroidal magnetic field diverges as $1/x$ as $x \rightarrow 0$, and hence its pressure diverges as $1/x^2$. Then, the vertical force due to the toroidal field pressure integrated over the top lid diverges logarithmically at small radii. To manage this singularity, we will modify the problem somewhat by introducing a small inner cut-off radius $R_{\text{in}} = x_{\text{in}} R_0$ of the tower, $x_{\text{in}} \ll 1$. This inner radius corresponds to the radius of the central jet that is embedded in the tower and that is actually responsible for carrying the axial line current. We use x_{in} as a small parameter to facilitate our analysis.

The contribution of the toroidal field pressure to the overall integrated vertical force,

$$F_z^{(B_\phi)} \equiv 2\pi R_0^2 \int_{x_{\text{in}}}^1 \frac{B_\phi^2}{8\pi} x dx = \frac{\Psi_0^2}{4R_0^2} \int_{x_{\text{in}}}^1 I^2(\psi) \frac{dx}{x}, \quad (63)$$

is dominated by the contribution near the cut-off radius; using the function $I(\psi)$ given by equation (57), this contribution can be estimated as

$$F_z^{(B_\phi)} = \frac{\lambda^2}{2} \frac{\Psi_0^2}{R_0^2} \int_{x_{\text{in}}}^1 \psi(x) d \log x \simeq \frac{\lambda^2}{2} \gamma B_0^2 R_0^2. \quad (64)$$

where we introduced a large parameter

$$\gamma \equiv |\log x_{\text{in}}| \gg 1. \quad (65)$$

Now, for what values of the parameters η and γ do solutions exist? To answer this question, we have used *Mathematica*

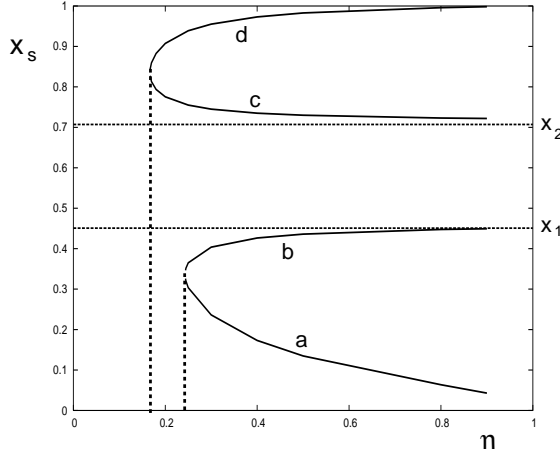


FIG. 6.— The position x_s of the separatrix as a function of η for the four solution branches corresponding to $x_{\text{in}} = 10^{-4}$ in our Case 2.

to map out the two-dimensional (η, γ) parameter space. We have restricted our investigation to $\gamma \gg 1$ and $\eta \leq 1$. We have found that the system exhibits a very rich mathematical behavior characterized by the multiplicity of solutions. The overall picture is illustrated in Figure 6, where we plot the separatrix position x_s as a function of η for a fixed value of $\gamma = 9.21$ (corresponding to $x_{\text{in}} = 10^{-4}$). We found that essentially there are two pairs of solutions, one pair corresponding to $x_s < x_2 = 2^{-1/2}$ and the other corresponding to $x_s > x_2$. When $\eta = 1$ there are only two solutions, one in each of these two regions. However, for $\eta < 1$ two more solutions appear, so there are four in total, with very different properties. As one decreases η at a fixed γ , the difference between the two solutions in each pair gradually diminishes, until they finally merge into one solution. As can be seen from Figure 6, this happens at two critical values of η , which we call $\eta_{\text{min},1}$ for the two solutions below x_2 and $\eta_{\text{min},2}$ for the two solutions above x_2 . We found that both $\eta_{\text{min},1}$ and $\eta_{\text{min},2}$ scale inversely with γ : $\eta_{\text{min},1}(\gamma) \approx 2.25\gamma^{-1}$, and $\eta_{\text{min},2}(\gamma) \approx 1.5\gamma^{-1}$. There are no solutions for $\eta < \eta_{\text{min},1,2}(\gamma)$.

As an illustration, we present the four solutions corresponding to $x_{\text{in}} = 10^{-4}$ ($\gamma = 9.21$) and $\eta = 0.3$ obtained using *Mathematica*. In Figure 7 we plot the vertical and toroidal components of the magnetic field for these solutions. One can see that the toroidal field goes to zero as $|x - x_s|^{1/2}$ on both sides of the separatrix without changing sign and grows as x^{-1} near the axis, which is explained by the assumed shape of the function $I(\psi)$. One can also notice that the vertical field in these solutions not only reverses sharply across the separatrix, but also changes sign by going smoothly through zero at one or two other points. This means that the magnetic field described by these solutions actually has a more complex topology than that of the simple tower of Figure 3. Thus, solutions 1c and 1d correspond to two towers, one inside the other, and solutions 1a and 1b corresponds to three nested towers.

The reason for the existence of two solutions with $x_s > x_2$ for $\eta > \eta_{\text{min},2}$ can be traced to the following argument. The vertical force (64) leads to a cocoon side pressure that scales as $\lambda^2 \gamma \eta B_0^2$. This pressure has to be balanced at the outer edge of the tower by the internal magnetic pressure that generally is of the order of $B_0^2/(1 - x_s)^2$. It turns out that, provided that $\eta > \eta_{\text{min},2}$, there are two ways to make such a balance, two different regimes, distinguished by whether x_s is close to 1 or

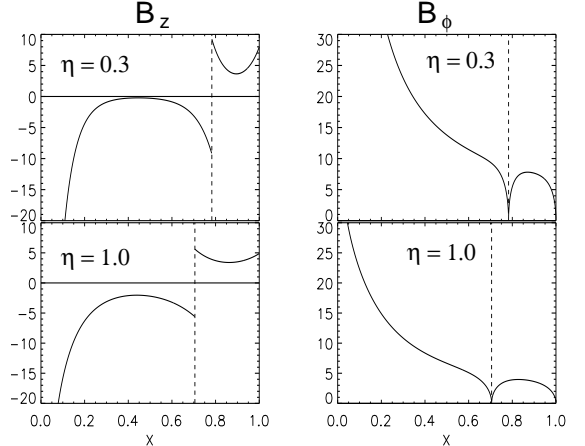


FIG. 7.— Vertical (left) and toroidal (right) magnetic field components of the four solutions in Case 2, computed for $x_{\text{in}} = 10^{-4}$ ($\gamma \simeq 9.2$) and $\eta = 0.3$. The vertical dashed lines on each plot shows the position x_s of the separatrix, across which the vertical field component (B_z) reverses sharply [the toroidal (B_ϕ) component is symmetric with respect to x_s].

not. We shall now consider these two possibilities (which we call Case 2c and Case 2d) separately and give basic analytical derivations under the assumption that $\eta\gamma \gg 1$ (and hence $\eta \gg \eta_{\text{min},2}$).

Case 2c: Let us assume that $x_s - 1$ is finite. Then, the force balance condition at the side wall of the tower can be satisfied only if λ is small, namely, $\lambda^2 \propto (\eta\gamma)^{-1}$. This suggests the following overall picture. Since λ^2 is the factor that parameterizes the general strength of the toroidal field pressure, we see that the toroidal field term $-II'(\Psi)$ in the Grad–Shafranov equation is unimportant in most of the tower, with the exception of a small vicinity of the inner edge. The field is then predominantly vertical almost everywhere; the force-free balance then dictates that this field must be essentially uniform in each of the two regions. Since the total upward-directed magnetic flux in region II must equal to the total downward-directed flux in region I, the areas of the two regions must then be the same, hence $x_s^2 \approx 1/2$. Then we can approximate x_s in equations (60)–(61) by $x_2 = 2^{-1/2}$ and rewrite them as

$$\psi^I(x) \simeq 1 - 2x^2, \quad (66)$$

$$\psi^{II}(x) \simeq 2x^2 - 1, \quad (67)$$

corresponding to $B_z^I(x) \simeq -4B_0$, and $B_z^{II}(x) \simeq 4B_0$.

Next, the overall integrated force F_z is the sum of the positive contribution $F_z^{(B_\phi)}$ of the toroidal field pressure near the axis and the negative contribution from the poloidal field tension in the rest of the tower:

$$F_z = F_z^{(B_\phi)} - \frac{1}{4} B_0^2 R_0^2 \int_{x_{\text{in}}}^1 \psi_x^2 \frac{dx}{x} \simeq \left(\frac{\lambda^2 \gamma}{2} - 2 \right) B_0^2 R_0^2. \quad (68)$$

Then, using the condition (45) of the pressure balance between the tower and the cocoon at the outer edge $x = 1$, we obtain a simple approximate expression for λ in terms of γ :

$$\lambda \simeq 2 \sqrt{\frac{1+\eta}{\eta\gamma}} \ll 1, \quad (69)$$

which reduces to $\lambda \simeq (8/\gamma)^{1/2}$ for $\eta = 1$ and $\lambda \simeq 2(\eta\gamma)^{-1/2}$ for $\eta \ll 1$. By combining this expression with the asymptotic

behavior

$$\lambda(x_s \rightarrow x_2) \simeq 4 \sqrt{\frac{\sqrt{2}}{1-\log 2}} \sqrt{x_s - 1/\sqrt{2}} \simeq 8.587 (x_s - 1/\sqrt{2})^{1/2}, \quad (70)$$

of the function $\lambda(x_s)$ [obtained from equation (62) in the limit $x_s \rightarrow x_2$], we can determine exactly how close x_s has to be to x_2 in terms of γ and η :

$$x_s - x_2 = \frac{1+\eta}{\eta\gamma} \frac{1-\log 2}{4\sqrt{2}} \simeq 0.054 \frac{1+\eta}{\eta\gamma}. \quad (71)$$

This becomes $x_s - x_2 \simeq 0.11\gamma^{-1}$ for $\eta = 1$ and $x_s - x_2 \simeq 0.054(\eta\gamma)^{-1}$ for $\eta \ll 1$.

Finally, by substituting equation (69) into (68) and using relationship (30), we get an estimate for the cocoon pressure at the top of the tower:

$$P_{\text{top}} \simeq \frac{2}{\pi\eta} B_0^2 \simeq \frac{0.637}{\eta} B_0^2, \quad (72)$$

which is of course consistent with the pressure balance across the side wall between the cocoon and the magnetic field $4B_0$ inside the tower. Equation (33) can then be used to estimate the tower's vertical expansion velocity:

$$V_{\text{top}} \simeq \sqrt{6/\eta} V_{A,0} \simeq 2.45 \eta^{-1/2} V_{A,0}. \quad (73)$$

This result, together with its counterpart from the previous example, indicates that V_{top} between 2.5 and 3 $V_{A,0}$ provides a more accurate estimate for the tower growth velocity than equation (10).

With these results at hand, we can go back and compute the differential rotation profile $\Delta\Omega(\psi)$ that corresponds to this case. As long as we are not too close to $\psi = 1$, we can use equations (66) and (67) to explicitly express $x_1(\psi)$ and $x_2(\psi)$ in terms of ψ and we can also approximate $\psi_x^I = -4x$, $\psi_x^{II} = 4x$. By substituting these approximations, along with (57), into equation (46), we get a very simple relationship

$$\begin{aligned} \Delta\Omega(\psi) &= \frac{\Delta\Phi}{t} = \sqrt{2}\lambda \frac{V_{A,0}}{R_0} \frac{\sqrt{\psi}}{1-\psi^2} \\ &\simeq \frac{4}{\sqrt{|\log x_{\text{in}}|}} \sqrt{\frac{1+\eta}{2\eta}} \frac{V_{A,0}}{R_0} \frac{\sqrt{\psi}}{1-\psi^2}. \end{aligned} \quad (74)$$

This expression breaks down near $\psi = 1$ as of course it should since the toroidal field's pressure becomes significant and modifies the poloidal field structure near the inner edge. Also note that the factor $\sqrt{2}\lambda \simeq 4|\log x_{\text{in}}|^{-1/2}$ that is in front of this expression, although formally vanishing in the limit $x_{\text{in}} \ll 1$, in reality is never very small; for example, it is equal to ≈ 1.1 for $x_{\text{in}} = 1 \times 10^{-6}$.

We have used *Mathematica* to obtain exact (i.e., without relying on the assumption $\gamma \gg 1$) solutions for this case for several values of η and γ . In particular, we found that, in the limit of large γ , the resulting γ -dependences of λ , the separatrix position x_s , and the pressure in the cocoon P_{top} at a fixed η are in a good agreement with the above simple estimates. In addition, Figure 7c shows the radial profiles of the vertical and toroidal magnetic field components inside the tower for a representative case $x_{\text{in}} = 0.0001$ and $\eta = 0.3$. One can see that the vertical field is indeed close to a constant $4B_0$ outside the separatrix and $-4B_0$ inside, as expected, although it deviates significantly from this constant close to the central axis.

Case 2d: Another interesting case is that corresponding to x_s being close to 1 and hence a large λ . Then, assuming that

the contribution (64) of the toroidal pressure to the integrated vertical force dominates over the poloidal field contribution (this assumption is valid as long as $\eta \ll 1$, as we shall show below), we can estimate the post-shock pressure at the tower top as

$$P_{\text{top}} = \frac{F_z^{(B_\phi)}}{\pi R_{\text{out}}^2} = \frac{\lambda^2}{2\pi} B_0^2 \gamma. \quad (75)$$

Applying the condition of pressure balance across $R = R_0$, we then get:

$$\frac{I_{\text{pol}}^2(\psi = 1)}{R_0^2} + \frac{\Psi_0^2}{R_0^4} \psi_x^2(x = 1) = 8\pi P_{\text{side}} = 8\pi\eta P_{\text{top}} = 4\lambda^2\gamma\eta B_0^2. \quad (76)$$

The contribution of the toroidal field to the pressure balance at the outer boundary is $B_\phi^2(x = 1) = I_{\text{pol}}^2(\psi = 1)/R_0^2 = 2\lambda^2 B_0^2$. Assuming that $\eta\gamma \gg 1$, we can therefore neglect it in comparison with $8\pi P_{\text{side}}$, and so the above pressure balance condition yields

$$\psi_x(x = 1) \simeq 2\lambda \sqrt{\gamma\eta}. \quad (77)$$

Now we want to use this relationship in conjunction with our general solution derived above to determine the parameter λ . Notice that the introduction of the inner radius does not alter the general functional form of $\psi(x)$ given by equation (59). The inner boundary condition is changed into $\psi(x_{\text{in}}) = 1$. However, we expect that, for $x_{\text{in}} \ll 1$, the relationships between the coefficients that describe the function $\psi(x)$ are changed only slightly, even though they had been derived using the boundary condition $\psi(x = 0) = 1$. Then, as long as we are not too close to the inner boundary, we can still use expressions (60)–(61) for our solution. In particular, we can write $\psi_x(x = 1)$ as

$$\psi_x(x = 1) = \frac{2}{1-x_s^2} - \lambda^2 \frac{x_s^2}{1-x_s^2} \log x_s - \frac{\lambda^2}{2}. \quad (78)$$

We can simplify this expression by noticing that the relationship (62) between λ and x_s can be cast in the form $\lambda^2 x_s^2 \log x_s = 2(2x_s^2 - 1) - \lambda^2 x_s^2(1-x_s^2)$. Then, the above expression for $\psi_x(x = 1)$ greatly simplifies and, substituting it into the pressure balance condition (77), we obtain

$$\psi_x(x = 1) = 4 + \lambda^2 \left(x_s^2 - \frac{1}{2} \right) = 2\lambda \sqrt{\gamma\eta}. \quad (79)$$

From this, we can express x_s in terms of λ as

$$x_s^2 = \frac{1}{2} + 2 \frac{\lambda\sqrt{\gamma\eta} - 2}{\lambda^2}. \quad (80)$$

This equation, together with equation (62), completely determines both x_s and λ for a given value of the product $\gamma\eta \gg 1$. We can go even further and get explicit formulae for x_s and λ by making use of the fact that $x_s \approx 1$ [and hence, according to eq. (62), $\lambda \gg 1$] in the regime under consideration. Then, the first term in (79) is small compared with the second term and we immediately obtain

$$\lambda \simeq 4\sqrt{\gamma\eta} \equiv 4\sqrt{\eta|\log x_{\text{in}}|} \gg 1, \quad (81)$$

and

$$|\log x_s| \simeq 1 - x_s \simeq \frac{2}{\lambda^2} \simeq \frac{1}{8\gamma\eta} \ll 1. \quad (82)$$

With these results, we can now go back to our solution given by equations (60)–(61) and derive the following asymptotic expressions for $\psi(x)$ in the two regions

$$\psi^I(x) \simeq 1 - 2x^2 - 8\gamma\eta x^2 \log x, \quad x \gg x_{\text{in}}; \quad (83)$$

$$\psi^{II}(x) \simeq 1 - 8\gamma\eta(1 - x^2 + x^2 \log x) \simeq 1 - 8\gamma\eta(1 - x). \quad (84)$$

From our estimations of the vertical force and the post-shock pressure above the tower, we find

$$F_z \simeq \frac{\gamma \lambda^2}{2} B_0^2 R_0^2 \simeq 8\gamma^2 \eta B_0^2 R_0^2, \quad (85)$$

and

$$P_{\text{top}} \simeq \frac{8\gamma^2}{\pi} \eta B_0^2. \quad (86)$$

Correspondingly, the vertical expansion speed is

$$V_{\text{top}} = \sqrt{\frac{3}{4} \frac{P_{\text{top}}}{\rho_0}} \simeq \sqrt{\frac{6\eta}{\pi}} \gamma \frac{B_0}{\sqrt{\rho_0}} = \sqrt{24\eta} \gamma V_{A,0} \gg V_{A,0}. \quad (87)$$

This suggests that magnetic tower configurations with a non-zero line current along the axis may be especially effective in producing jets that are rapidly propagating through a confining external medium.

As a final check, we now go back to our estimate of the integrated vertical force and ask under what circumstances it is indeed dominated by the toroidal field contribution. Using our solution (83)–(84) and assuming that $\gamma\eta \gg 1$, the poloidal field contribution can be estimated as $F_z^{(B_z)} \simeq -8\gamma^2 \eta^2 B_0^2 R_0^2$, whereas, substituting (81) into equation (64), one estimates the toroidal field contribution to be $F_z^{(B_\phi)} \simeq 8\gamma^2 \eta B_0^2 R_0^2$. Thus, we see that $F_z^{(B_\phi)}$ indeed dominates as long as $\eta \ll 1$.

5. DISCUSSION

5.1. Transition to the Relativistic Expansion Regime and the Final Opening Angle of the Jet

[In general, we have to distinguish between relativistic expansion velocity and the relativistic field-line rotation velocity ($R_0 \gg R_{LC}$) inside the tower. In our non-relativistic analysis these two velocities are comparable, but it is not going to be so in the relativistic case. In addition to the expansion velocity, there is the issue of relativistic rotation of field lines inside the tower. This happens when the radius of the tower is larger than the light cylinder so that $\Omega R_0 \gg c$.]

As we have shown in § 2.2, the radius R_0 of the tower, and hence the rotational velocity of the field lines and the tower's growth velocity $V_{\text{top}} \sim \Delta\Omega R_0$ scale with the background density as $\rho_0^{-1/6}$. Therefore, as the tower expands into the outer, less dense regions of the star, V_{top} inevitably reaches the speed of light at a certain point that corresponds to some critical density $\rho_{0,\text{rel}}$. Our non-relativistic model becomes invalid at this point and any further expansion of the tower requires a relativistic treatment. For our fiducial values $B_d = 10^{15}$ G, $R_d = 3 \cdot 10^6$ cm, and $\Delta\Omega = 3 \cdot 10^3$ sec $^{-1}$, this transition to the relativistic regime takes place at a critical density $\rho_{0,\text{rel}} \sim 10^6$ g/cm 3 [see eq. (18)]. For a typical massive stellar GRB progenitor this density corresponds to a distance Z_{rel} from the center that is on the order of a few times 10^8 cm; according to equation (16), the radius of the tower corresponding to this critical density is $R_{\text{rel}} \sim 10^7$ cm.

A relativistic generalization of the magnetic tower model is beyond the scope of this paper but is something we intend to develop in the near future. Before a complete solution is achieved, however, we cannot really say anything definite about further expansion of the tower. However, we can, perhaps, look at the results of fully-relativistic hydrodynamic simulations (Zhang et al. 2003) for some physical insight. In those simulations the relativistic jet remained collimated as it propagated through the star, across several orders of magnitude in stellar density. The authors of that paper have attributed the observed collimation to recollimation

shocks in the cocoon and to relativistic beaming in the jet. But the physical processes in the cocoon should not change if we replace the inner relativistic hydrodynamic jet with a relativistic magnetic tower. Furthermore, we expect some additional, magnetic collimation due to the toroidal-field hoop stress (the pinch effect). The bottom line is that we expect the magnetic tower to remain well collimated even after it transitions into the relativistic regime. In particular, we suggest that the final opening angle of the magnetically-dominated outflow will be no larger than the inverse aspect ratio of the tower at the moment of relativistic transition:

$$\Delta\theta \lesssim \frac{R_{0,\text{rel}}}{Z_{\text{rel}}} \simeq 0.1. \quad (88)$$

Whether this prediction is true will have to be determined by a fully-relativistic analysis and by relativistic MHD simulations, which we hope will be completed in the near future. In addition, we acknowledge that some first steps toward developing an analytical understanding of magnetically-dominated outflows in the ultra-relativistic regime were taken recently by Lovelace & Romanova (2003) and by Lyutikov (2006).

5.2. Tower Structure

Figure 4 shows the run of vertical and azimuthal magnetic field components for Case 1 as a function of scaled radius x . For the $\eta = 1.0$ case (bottom panel), the toroidal field scales as $x^{-1/2}$ so that the enclosed toroidal magnetic energy increases linearly with radius. The toroidal magnetic energy is not concentrated toward the axis, but is distributed throughout the tower. For Case 2 with a central line current (Figure 7), however, the toroidal magnetic field increases toward the axis ($x = 0$) as x^{-1} . The magnetic energy density is thus strongly peaked toward the axis for this case. This demonstrates that the presence of a central line current results in a more tightly beamed outflow.

For the field structures of Case 2 plotted in Figure 7 we found solutions corresponding to multiple nested towers. Case 2c, for example, has B_z passing through 0 at $x \sim 0.1$ and a separatrix at $x \sim 0.75$ corresponding to two distinct towers, one within the other. Field lines in the inner tower are tied to the disk deeper in the potential of the black hole or neutron star where the characteristic velocity becomes comparable to the speed of light. Thus, the inner tower may be a more energetic component of the outflow and may reach the ultra-relativistic expansion regime earlier. In addition, the inner tower is shielded from the cocoon material by the outer tower which envelopes it. This is beneficial for achieving relativistic flow in the inner tower since baryon contamination is suppressed. We note that, in principle, the tops of the towers can propagate at different speeds, as indicated schematically by the tower heights in Figure 8. However, we have not analyzed this case in detail since all analysis we present here assumes a single tower height.

5.3. Baryon Contamination from the Disk

The tower plasma may be polluted with baryons from the disk by two main processes, magneto-centrifugal acceleration (Blandford & Payne 1982) and radiative neutrino-driven ablation (Qian & Woosley 1996). In the case of magneto-centrifugal acceleration, the field lines must be inclined outward by at least 30 degrees from vertical for a disk wind to be launched. It is of interest to note that, for our configuration, field lines forming the inner tower are plausibly constrained to leave the disk at progressively steeper angles, moving inward

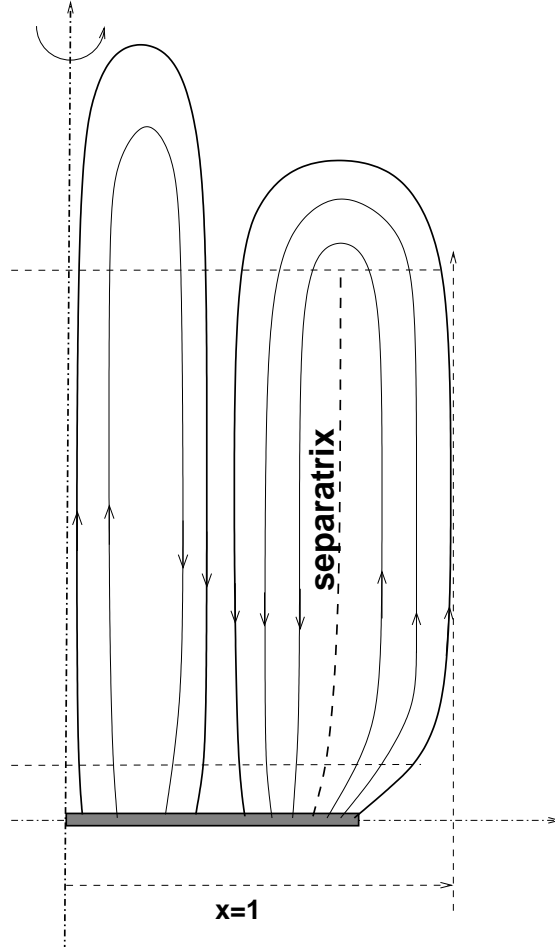


FIG. 8.— A schematic drawing of a twin magnetic tower. The outer tower which forms a hollow cylindrical shell which surrounds the inner tower.

toward the rotation axis. This field configuration would suppress the magneto-centrifugal launching mechanism for the inner tower. The outer tower may be more baryon loaded than the inner tower and would constitute a less relativistic magnetically dominated flow at larger angles from the pole. Yet farther from the pole, the cocoon represents an even higher baryon loaded component and is consequently expected to be slower and contain a relatively small magnetization (whatever magnetic field is mixed into the cocoon by plasma instabilities). Future relativistic magnetohydrodynamical simulations will be able to address these issues and in particular determine the angle of field lines emerging from the inner disk enabling better estimates of baryon contamination. In addition, we note that in the case of black hole–disk magnetic coupling, one should expect no baryon loading at all along the part of a field line that connects to the black hole, as has also been pointed out by e.g. Levinson & Eichler (1993).

Some baryons are expected to be driven into the tower (along field lines attaching to the disk) by neutrino ablation. As of yet, no detailed calculations of neutrino-driven ablation exist for collapsar disks. For example, neutrinos may escape the disk in hot magnetically dominated bubbles without advecting large numbers of baryons into the tower. In addition, Vlahakis et al. (2003) argued that neutrons, which may constitute the majority of the baryons in the disk wind, are not subject to electromagnetic acceleration and hence decouple

from the relativistic outflow at rather moderate Lorentz factors; this significantly lessens the baryon pollution expected from the disk wind.

5.4. Effect of MHD Instabilities on the Tower Evolution

One of the most serious uncertainties in the magnetic tower model is the stability of this highly twisted structure. In this section we discuss the effects that ideal MHD instabilities may have on the magnetic tower in the collapsar context. A scenario involving reconnection inside the tower due to finite resistivity will be discussed in the next section.

Indeed, as the tower grows, it becomes very elongated and hence prone to a number of ideal MHD instabilities. Among the most obvious instability candidates are:

(i) Rayleigh–Taylor (or, perhaps more relevant, Richtmyer–Meshkov) instability taking place at the tower’s top. This may cause splitting of the magnetic tower into a number of separate strands interleaved with regions filled with stellar matter.

(ii) Kelvin–Helmholtz instability at the side boundary between the tower and the cocoon, leading to entrainment of the baryonic stellar material into the tower. This instability however should be stabilized by the strong vertical magnetic field in the tower.

(iii) A non-axisymmetric ideal-MHD kink-like instability taking place in the main body of the tower. Although this problem has not been studied in the magnetic-tower context, it has been considered in the framework of relativistic force-free electrodynamics for field lines connecting a disk to a black hole (Gruzinov 1999). In addition, an important clue can be derived from stability studies of regular MHD jets. For example, a recent numerical investigation of non-relativistic Poynting-flux dominated jets propagating through an stratified external medium indicated that jet stability strongly depends on the background density profile; in particular, the system is found to be stable if the density decreases fast enough along the jet (Nakamura & Meier 2004).

If it does go unstable, the kink is probably the most dangerous instability that may lead, in the nonlinear phase, to a significant, although perhaps temporary, disruption. Such a disruption, however, is not necessarily a bad thing: the tower may be able to reform after being disrupted (as is seen in laboratory experiments by Lebedev et al. 2005) and the resulting non-steady evolution may provide a plausible mechanism for rapid variability seen in gamma-ray bursts.

We also would like to point out that, as one expected outcome of the nonlinear development of an MHD instability, a significant fraction of the toroidal magnetic field energy may be dissipated into thermal energy (Eichler 1993; Begelman 1998). Importantly, this process may occur somewhere inside the tower, way above the inner accretion disk. Since the plasma density in the tower is very low, this may have an additional beneficial side-effect on the explosion dynamics due to the possibility of non-thermal neutrino emission coming from the magnetic dissipation sites. The resulting high-energy neutrinos are expected to have better coupling to baryonic stellar matter, thus providing an extra source for the strong shock propagating through the star (Ramirez-Ruiz & Socrates 2005). In addition, as has been shown by Drenkhahn & Spruit (2002; see also Giannios & Spruit 2006), magnetic energy dissipation may also have a positive influence on the acceleration of the Poynting-flux dominated outflow.

So far as we know, there have been no formal stability studies of magnetic towers to date. Such studies are clearly needed. They may involve a linear perturbation analysis or

a non-axisymmetric MHD simulation. Such stability studies should take into account several stabilizing effects. First, the magnetic tower is not in a vacuum, but is being confined by a high-pressure cocoon. The cocoon may provide some stabilization at least for external kink modes, although internal kink modes will not be affected. Some theoretical evidence supporting the idea of the external pressure stabilization can be derived from Königl & Choudhuri's (1985) analysis of a force-free magnetized jet that confined by an external pressure. Indeed, they showed that a non-axisymmetric helical equilibrium state becomes energetically favorable (conserving the total magnetic helicity in the jet) only when the pressure drops below a certain critical value. If this happens and the external kink does go unstable, then this non-axisymmetric equilibrium may perhaps be interpreted as the end point of the non-linear development of the instability.

A second important stabilizing factor, discussed earlier in this section, is the expectation that the tower should quickly transition to the relativistic regime. Once the outflow becomes ultra-relativistic with a very large γ -factor, the relativistic time delay may effectively stabilize the tower (Giannios & Spruit 2006). The reason for this is that MHD instabilities grow on the local Alfvén-crossing time in the fluid frame and hence much slower in the laboratory frame. As a result, even if instabilities are excited, they do not have enough time to develop before the break-out of the flow from the star.

5.5. Reconnection Inside the Tower

Another important process that may affect the propagation of the magnetic tower through the star is magnetic reconnection across the cylindrical separatrix current sheet at $R = R_s$. This process could, in principle, lead to the break up of a single tower into a train of smaller spheromak-like plasmoids. Instead of a further lengthening of the tower, one would then effectively get continuous injection of new plasmoids at the base of the outflow. The new plasmoids would push the existing ones further up the axis, so that the net dynamical effect would probably be essentially the same as that of one single continuously growing tower. The physics of this process is in fact identical to the cyclic generation of plasmoids via reconnection across the separatrix suggested in the context of magnetospheres of accreting young stars, resulting in a knotty jet (Goodson et al. 1999; see also Uzdensky 2004). At what level this tearing instability should saturate, i.e., what should be the expected size of the plasmoids, is presently not known.

We would like to remark, however, that we doubt that a fast and efficient reconnection process is possible in the tower, as long as it is still deep inside the star. It is indeed true that fast reconnection is commonly believed to be the underlying mechanism for many spectacular and most energetic astrophysical phenomena, from substorms in the Earth magnetosphere, to flares in the solar corona (e.g., Sweet 1958), to X-ray flares in magnetars (Lyutikov 2003). However, all these cases are characterized by relatively low-density environments, where classical collisional resistivity is so small that other, non-classical terms in the generalized Ohm law (i.e., the Hall term or anomalous resistivity) become important. This happens when the reconnection layer thickness, computed from the classical Sweet-Parker theory (Sweet 1958; Parker 1957) with Spitzer resistivity, becomes smaller than the relevant microscopic plasma length scales, such as the collisionless ion skin depth and/or the ion gyro-radius. This condition is easily satisfied both in the solar corona and in the Earth magnetosphere. Then, as many numerical simulations

(e.g., Mandt et al. 1994) have shown, reconnection proceeds at a fast rate, in part due to the so-called Petschek mechanism (Petschek 1964).

However, in the dense collapsar environment the situation is different. Even if the plasma pressure inside the magnetic tower constitutes a tiny but finite fraction of the magnetic pressure, the resulting electron-positron pair density is so high that the plasma should be considered strongly collisional. For example, let us assume, as an illustration, that the interior of the tower is filled with an optically-thick radiation-pressure dominated pair plasma with the thermal energy density equal to 10^{-3} of the magnetic energy density and let us make some simple estimates relevant to reconnection physics. For a characteristic magnetic field strength of 10^{14} G, the corresponding plasma temperature should be of order $T \sim 3 \cdot 10^9$ K $\simeq 300$ keV. The corresponding equilibrium pair density [using the non-relativistic formula $n_e = 2(m_e k_B T / 2\pi\hbar^2)^{3/2} \exp(-m_e c^2 / k_B T)$ for a rough estimate] is on the order of $n_e \sim 2 \cdot 10^{29}$ cm $^{-3}$. The classical non-relativistic Spitzer resistivity due to electron-positron collisions at the above temperature is $\eta \sim 0.1$ cm 2 /sec. Now, the main dimensionless quantity that characterizes the reconnection layer in resistive MHD regime is the Lundquist number $S \equiv V_A L / \eta$, where L is the global length-scale of the reconnecting system. Taking $L = 10^7$ cm and using the speed of light instead of the Alfvén velocity, we get $S \sim 3 \cdot 10^{18}$. Then, the classical Sweet-Parker reconnection theory gives us an estimate for the thickness of the reconnection layer as small as $\delta_{SP} = LS^{-1/2} \sim 6 \cdot 10^{-3}$ cm. This thickness is of course tiny compared with L , but it is huge compared with the relevant physical plasma length-scales, such as the electron collisional mean free path ($l_{mfp} \sim 10^{-6}$ cm), the electron gyro-radius ($\rho_e \sim 10^{-11}$ cm), and the electron collisionless skin-depth ($d_e \equiv c/\omega_{pe} \sim 10^{-9}$ cm). This means that, although they are themselves very small, the classical collisional resistivity (due to $e^+ - e^-$ Coulomb collisions) and the Compton drag (due to $e^+ - \gamma$ and $e^- - \gamma$ collisions) greatly exceed the collisionless terms in the generalized Ohm law. Therefore, resistive MHD (augmented by the Compton drag which may give a comparable, perhaps even somewhat larger than Spitzer, contribution to the total resistivity) should provide an accurate description of the plasma, even inside a very thin reconnection layer.

During the past two decades it has been convincingly demonstrated, via numerical simulations (e.g., Biskamp 1986; Uzdensky & Kulsrud 2000), theoretical analysis (Kulsrud 2001; Malyshkin et al. 2005), and laboratory plasma experiments (Ji et al. 1999), that in collisional resistive-MHD systems reconnection proceeds in the very slow Sweet-Parker regime and that the Petschek fast reconnection mechanism is disabled. If we can extend this result to the highly relativistic and optically-thick electron-positron plasma inside the collapsar magnetic tower, we then have to conclude that any large-scale reconnection across the separatrix is very slow and inefficient. One has to be aware of several caveats, however. First, the role of the photon drag on reconnection dynamics is not known, especially its effect on the geometry of reconnecting flow. Second, there is a possibility that, even in the resistive-MHD regime, reconnection can be greatly enhanced in the presence of MHD turbulence, as suggested by Lazarian & Vishniac (1999). And third, since magnetic energy density in the tower greatly exceeds both the plasma pressure and its rest-mass energy density, reconnection flow is bound to

be strongly relativistic; then special-relativistic effects, such as the Lorentz contraction, may modify the conclusions derived from the non-relativistic reconnection theory (Blackman & Fields 1994; Lyutikov & Uzdensky 2003). With all these reservations in mind, we still believe that reconnection processes are strongly inhibited in the tower when it is still deep inside the collapsing star. However, as the tower grows and eventually breaks out of the star, the plasma cools and the particle density in it drops rapidly. Therefore, we should expect that the plasma will become collisionless, at least as far as reconnection physics is concerned, at late times, perhaps after the break-out. This opens up the possibility that any possible disruption of the tower through reconnection (and corresponding magnetic energy release) is delayed and happens only after the tower clears the stellar surface.

5.6. Prospects for Numerical Simulations

In this paper we have developed a mathematical framework describing a sequence of static force-free equilibria which represents a magnetic tower inside a star. To verify if our picture is realizable in practice and to make further progress in understanding the development and evolution of magnetic towers in stars, it is desirable to perform time-dependent numerical simulations. Such simulations will determine the degree to which the simplifications we have adopted for our analytic model hold in realistic environments. The key feature to be investigated is the structure of the tower and the cocoon and how they may be affected by instabilities.

We envision a sequence of numerical simulations in which increasingly realistic physics is incrementally added to the simplest elemental simulation. Each of these studies will be able to answer a subset of key questions with increasing degree of realism. First, the following questions can be addressed with non-relativistic axisymmetric MHD simulations. What basic magnetic field configuration results, in practice, when the conditions we describe are set up? Under what conditions does a magnetic tower form, if at all? How do the tower growth and structure change as the tower expands into regions of lower density? To what degree is cocoon material mixed into the tower, and magnetic field from the tower mixed into the cocoon? How strongly is magnetic field concentrated toward the axis? How does the Poynting flux depend on radius and height? What is the overall field line geometry? Is magneto-centrifugal acceleration from the base of the outflow inhibited? In simulations where multiple towers are investigated, how do they interact? To what degree does the cocoon help collimate and stabilize the tower? How rapidly do the cocoon walls spread laterally? Can the cocoon expansion result in the disruption of the star? What differences are there between cocoons formed by purely hydrodynamical jets and by magnetic towers?

Next, relativistic MHD simulations will be able to address fundamental questions of critical interest to the application of magnetic towers to gamma-ray bursts. Of particular interest is the beaming angle and angular distribution of energy, Lorentz factor and magnetic field after the tower makes the transition to relativistic expansion and when it eventually breaks out of the stellar surface. Do relativistic effects suppress the growth of instabilities in the tower and surrounding plasma? In addition, inclusion of relativity is necessary for some regions of the central engine, e.g. outside of a magnetar light cylinder or the inner parts of black hole accretion disks.

Finally, three-dimensional simulations, both relativistic and non-relativistic, will enable study of non-axisymmetric insta-

bilities. Intermixing of baryonic material and magnetic field between the tower and the cocoon may also be quantitatively addressed with three-dimensional simulations.

Several numerical schemes have recently been developed (Koide, Shibata, & Kudoh 1999; Gammie, McKinney & Tóth 2003; Del Zanna, Bucciantini, & Londrillo 2003; De Villiers, Hawley & Krolik 2003; Fragile 2005; Komissarov 2005; Nishikawa et al. 2005) which should be capable of simulating magnetic towers powered by central engines formed after core collapse. In fact, general relativistic MHD simulations of collapsars have already been performed by two groups (Mizuno et al. 2004; De Villiers, Staff, & Ouyed 2005). In principle these simulations may contain structures which could be termed magnetic towers as described in this paper. However, it may be difficult to clearly discern the properties of the magnetic structure in complex simulations. For this reason we suggest above incremental simulations guided by analytic studies as presented here.

While the magnetic tower itself is force-free, pressure and inertia of the surrounding plasma play a key role in its development. This points to the desirability of magnetohydrodynamical (MHD) simulations capable of simultaneously solving force-free and hydrodynamical regions of the flow. One possible choice is a hybrid numerical scheme which solves relativistic force-free equations in highly magnetized parts of the computational domain, e.g. within the tower, with a moving contact discontinuity evolved within a hydrodynamical simulation (Blandford 2005, private communication).

As an ultimate goal, numerical simulations of the full problem, including a detailed description of the central engine with relevant microphysical processes and neutrino transport, are desirable for a comprehensive understanding of the formation and evolution of a magnetic tower in a star.

6. CONCLUSIONS

In this paper we have proposed a new mechanism for driving a strongly-collimated, baryon-poor, magnetically-dominated outflow through a massive star in the collapsar model (e.g., MacFadyen & Woosley 1999) for long-duration gamma-ray bursts. This magnetic mechanism may work independently and in parallel with the usual neutrino-driven outflow mechanism. It may also be relevant for asymmetric core-collapse supernova explosions.

To model the magnetically-dominated outflow, we invoke the concept of the magnetic tower, first introduced by Lynden-Bell (1996) in the AGN context. Overall, our model can be outlined as follows. The core collapse of a massive rotating star may result in two distinct configurations, both plausible candidates for the GRB central engine. The first one is a stellar mass black hole accreting rapidly through an accretion disk. The second is a millisecond magnetar. A hybrid configuration with a disk around a magnetar is also possible. In the first case, the core of a rotating massive star collapses into a black hole (or forms a proto-neutron star), whereas the overlying stellar material that is continuously falling towards the center may possess enough angular momentum to form an accretion disk. Any pre-existing stellar magnetic field becomes greatly amplified by the combined action of compression during the collapse and field-line stretching due to differential rotation. In addition, the disk is generally unstable to magneto-rotational instability (MRI) and becomes turbulent. This results in further amplification of the magnetic field due to turbulent dynamo action inside the disk, up to the level that may be in excess of 10^{16} G (as suggested by Akiyama et al.

2003 in the core-collapse supernova context). Even though this field is predominantly toroidal, the poloidal field component may also be significant; we believe that a figure of 10^{15} G for the large-scale poloidal magnetic field is not unreasonable.

As a result of the amplification, magnetic tubes become buoyant and escape out of the disk into the overlying low-density corona, forming coronal loops. These loops are anchored at both ends at the disk surface but, generally speaking, the two footpoints of a loop are at different distances from the center and hence rotate at different angular velocities. The resulting differential rotation further twists the magnetic loops, generating more toroidal flux, and the disk magnetosphere tends to inflate. A similar process has also been shown to work in the case of a magnetic field linking the disk directly to the black hole (Uzdensky 2005). In any case, it is this inflation process that is ultimately responsible for the formation of the magnetically-dominated outflow in our model. For simplicity, we consider the evolution of an axisymmetric magnetic arcade. Because the density in the corona above the disk is low, the initial expansion is force-free and takes place at some finite angle with respect to the rotation axis. Subsequently, however, the expanding magnetic field weakens to such a degree that it starts to feel the presence of the ambient stellar gas. As was shown by Lynden-Bell (1996), any external gas pressure surrounding an expanding twisted magnetic arcade eventually becomes dynamically important and channels the expansion into the vertical direction; a tall magnetic tower forms and continuously grows as a result. In our model, we modify Lynden-Bell's model by taking into account that the tower expansion is supersonic with respect to the unperturbed stellar gas. We thus envision the growing magnetic tower acting as a piston that drives a strong shock through the star. The hot shocked stellar material between the shock and the tower forms a high-pressure cocoon, similar to that seen in hydrodynamic simulations by Zhang et al. (2003). This cocoon envelopes the tower and provides the collimating pressure for it. Thus, in our model, the tower is confined not by the pressure of the background stellar material, but by its inertia; the strong shock and the cocoon act as mediators that convert the inertial support into the pressure support that ultimately acts on the tower.

The entire configuration grows vertically with time and eventually reaches the star's surface, thus providing a very narrow baryon-clean channel in the form of a Poynting-flux dominated jet, surrounded by a less-collimated hot gas outflow. One of the great advantages of the magnetic tower model in the GRB context is that the magnetic field lines remain closed (e.g., with both ends tied to the disk) during the expansion process and, as a result, the volume occupied by the tower remains insulated from the surrounding stellar gas and hence relatively baryon-free. As the tower grows, it just pushes the stellar gas out of its way into the cocoon.

In addition, we believe that the physical scenario developed in this paper may also be applicable to the case where the central engine is a rapidly-rotating (i.e., millisecond) magnetar. The rotational energy of the magnetar is extracted magnetically as a Poynting flux that inflates a baryon-free cavity inside the progenitor star. This mechanism is similar to that proposed by Ostriker & Gunn (1971) for powering type II supernovae. However, whereas their model was spherically-symmetric, we suggest that a relativistic generalization of the magnetic tower model can naturally result in splitting of the magnetically-dominated outflow into a pair of oppositely directed narrow jets.

In our paper we first give a simple description of Lynden-Bell's magnetic tower model in its original accretion disk context (§ 2.1). Then we present our model of a magnetic tower propagating and driving a shock through a star (§ 2.2). We derive some basic scalings for the tower parameters (§ 2.3) and make some simple estimates for them (§ 2.4). Then, in § 3–4, we illustrate our model by two specific analytical solutions for the magnetic field structure in the main body of the tower; one of the solutions (§ 4.2) is characterized by a very narrow axial jet with a non-zero poloidal line current present in the core of the tower. In § 5 we briefly discuss several interesting physical issues that, although important, lie beyond the scope of the present paper. Namely, in § 5.1 we argue that, even though it may start off non-relativistically, the expansion of the tower will quickly have to transition to the relativistic regime. In § 5.3 we discuss the issue of baryon contamination of the tower by disk winds. Next, in § 5.4 we touch upon the question of stability of the magnetic tower configuration and address the role that ideal MHD instabilities may play in our scenario. In § 5.5 we discuss the possibility of the tower disruption and its break-up into a series of smaller plasmoids via internal reconnection. We argue, however, that, while the tower is still deep inside the star, the plasma inside of it is likely to be strongly collisional, so that classical resistive-MHD should apply inside the reconnection region. If this is the case, then, we believe, any reconnection process should be very slow, and so a global disruption through reconnection is not likely during this stage. During subsequent expansion, however, the density drops and the reconnection process may enter a faster collisionless regime, perhaps resulting in rapid magnetic energy dissipation.

Finally, in accordance with our discussion in § 5, we can formulate the following three areas that, we believe, require immediate attention and should and can be addressed in the near future. They are: (1) a special-relativistic generalization of the magnetic tower model; (2) 3D relativistic MHD numerical simulations of a magnetic tower inside a star; (3) the conditions for and the non-linear development of, various MHD instabilities.

We are grateful to ... for stimulating discussions. We thank the Kavli Institute for Theoretical Physics at UC Santa Barbara for its hospitality during the program on the Physics of Astrophysical Outflows and Accretion Disks in 2005 where part of this research was conducted. AIM acknowledges support from the Keck Fellowship at the Institute for Advanced Study. DAU's research has been supported by the National Science Foundation under Grant PHY-0215581 (PFC: Center for Magnetic Self-Organization in Laboratory and Astrophysical Plasmas).

REFERENCES

- Akiyama, S., Wheeler, J. C., Meier, D. L., & Lichtenstadt, I. 2003, *ApJ*, 584, 954
- Begelman, M. C. 1998, *ApJ*, 493, 291
- Begelman, M. C., Blandford, R and Rees, M., *Review of Modern Physics* 1984, 56, 255
- Biskamp, D. 1986, *Phys. Fluids*, 29, 1520
- Blackman, E. G. & Field, G. B. 1994, *Phys. Rev. Lett.*, 72, 494
- Blandford, R. D., & Payne, D. G. 1982, *MNRAS*, 199, 883
- Blandford, R. D. & Znajek, R. L. 1977, *MNRAS*, 179, 433
- Del Zanna, L., Bucciantini, N., & Londrillo, P. 2003, *A&A*, 400, 397
- De Villiers, J.-P., Hawley, J. F., & Krolik, J. H. 2003, *ApJ*,

599, 1238

De Villiers, J.-P., Staff, J., & Ouyed, R. 2005; preprint (astro-ph/0502225)

Drenkhahn, G., & Spruit, H. 2002, A&A, 391, 1141

Eichler, D. 1993, ApJ, 419, 111

Fragile, P. C., 2005, preprint (astro-ph/0503305)

Fryer, C. L., & Heger, A. 2005, ApJ, 623, 302

Fukuda, I. 1982, PASP, 94, 271

Galama, T. J. et al. 1998, Nature, 395, 670

Gammie, C. F., McKinney, J. C., & Tóth, G. 2003, ApJ, 589, 444

Giannios, D., & Spruit, H. 2006, accepted to A&A; preprint (astro-ph/0601172)

Goodman, J., Dar, A., & Nussinov, S. 1987, ApJ, 314, L7

Goodson, A. P., Böhm, K.-H., & Winglee, R. M. 1999, ApJ, 524, 142

Gruzinov, A., 1999, preprint (astro-ph/9908101)

Harrison, F. A. et al. 1999, ApJ, 523, L121

Heger, A., Woosley, S. E., & Spruit, H. C. 2005, ApJ, 626, 350

Hjorth, J. et al. 2003, Nature, 423, 847

Hsu, S. & Bellan, P. M. 2002, MNRAS, 334, 257

Lebedev, S. V., Ciardi, A., Ampleford, D. J., Bland, S. N., Bott, S. C., Chittenden, J. P., Hall, G. N., Rapley, J., Jennings, C. A., Frank, A., Blackman, E. G., & Lery, T. 2005, MNRAS, 361, 97

Hirschi, R., Meynet, G., & Maeder, A. 2005, A&A, 443, 581

Ji, H., Yamada, M., Hsu, S., Kulsrud, R., Carter, T., & Zdziarska, S. 1999, Phys. Plasmas, 6, 1743

Kato, Y., Hayashi, M. R., & Matsumoto, R. 2004, ApJ, 600, 338

Koide, S., Shibata, K., & Kudoh, T. 1999, ApJ, 522, 727

Komissarov, S. S. 2005, MNRAS, 359, 801

Königl, A. & Choudhuri, A. R. 1985, ApJ, 289, 173

Kulsrud, R. M. 2001, Earth, Planets and Space, 53, 417

Kulsrud, R. M. 2005, Plasma Physics for Astrophysics, (Princeton: Princeton Univ. Press)

Lazarian, A. & Vishniac, E. T. 1999, ApJ, 517, 700

Lee, H. K., Wijers, R. A. M. J., & Brown, G. E. 2000, Phys. Reports, 325, 83

Lei, W.-H., Wang, D.-X., & Ma, R.-Y. 2005; ChJAA, 5, Suppl., 279

Levinson, A. & Eichler, D. 1993, ApJ, 418, 386

Li, H., Lovelace, R. V. E., Finn, J. M., & Colgate, S. A. 2001, ApJ, 561, 915

Lovelace, R. V. E., Romanova, M. M., & Bisnovatyi-Kogan, G. S. 1995, MNRAS, 275, 244

Lovelace, R. V. E. & Romanova, M. M. 2003, ApJ, 596, L159

Lynden-Bell, D. & Boily, C. 1994, MNRAS, 267, 146

Lynden-Bell, D. 1996, MNRAS, 279, 389

Lynden-Bell, D. 2003, MNRAS, 341, 1360

Lyutikov, M. & Uzdensky, D. 2003, ApJ, 589, 893

Lyutikov, M. & Blandford, R. 2003; preprint (astro-ph/0312347)

Lyutikov, M. 2004; preprint (astro-ph/0409489)

Lyutikov, M. 2006 to appear in the New Journal of Physics; preprint (astro-ph/0512342)

MacFadyen, A. I. & Woosley, S. E. 1999, ApJ, 524, 262

MacFadyen, A. I., Woosley, S. E., & Heger, A. 2001, ApJ, 550, 410

Maeder, A., & Meynet, G. 2005, A&A, 440, 1041

Malesani, D., et al. 2004, ApJL, 609, L5

Malyshkin, L. M., Linde, T., & Kulsrud, R. M. 2005, Phys. Plasmas, 12, 102902

Mandt, M. E., Denton, R. E., & Drake, J. F. 1994, Geophys. Res. Lett., 21, 73

McKinney, J. C. 2005, ApJ, 630, L5

Meszaros, P. & Rees, M. J. 1997, ApJ, 482, L29

Mizuno, Y., Yamada, S., Koide, S., & Shibata, K. 2004, ApJ, 615, 389

Nakamura, M. & Meier, D. L. 2004, ApJ, 617, 123

Nishikawa, K.-I., Richardson, G., Koide, S., Shibata, K., Kudoh, T., Hardee, P., & Fishman, G. J. 2005, ApJ, 625, 60

Ostriker, J. P. & Gunn, J. E. 1971, ApJ, 164, L95

Paczynski, B. 1998, ApJ 494, L45

Parker, E. N. 1957, J. Geophys. Res., 62, 509

Petschek, H. E. 1964, AAS-NASA Symposium on Solar Flares, (National Aeronautics and Space Administration, Washington, DC, 1964), NASA SP50, 425.

Petrovic, J., Langer, N., Yoon, S.-C., & Heger, A. 2005, A&A, 435, 247

Proga, D., MacFadyen, A. I., Armitage, P. J., & Begelman, M. C. 2003, ApJ, 599, L5

Proga, D. & Zhang, B. 2006, submitted to ApJ Letters; preprint (astro-ph/0601272)

Qian, Y.-Z., & Woosley, S. E. 1996, ApJ, 471, 331

Ramirez-Ruiz, E., & Socrates, A. 2005, preprint (astro-ph/0504257)

Soderberg, A. M., et al. 2006, ApJ, 636, 391

Stanek, K. Z., Garnavich, P. M., Kaluzny, J., Pych, W., & Thompson, I. 1999, ApJ, 522, L39

Stanek, K. Z. et al. 2003, ApJ, 591, L17

Sweet, P. A. 1958, in Electromagnetic Phenomena in Cosmical Physics, ed. B. Lehnert, (New York: Cambridge Univ. Press), 123

Thompson, C. 1994, MNRAS, 270, 480

Thompson, T. A., Chang, P., & Quataert, E. 2004, ApJ, 611, 380

Usov, V. V. 1992, Nature, 357, 472

Uzdensky, D. A. & Kulsrud, R. M. 2000, Phys. Plasmas, 7, 4018

Uzdensky, D. A., Königl, A., & Litwin, C. 2002, ApJ, 565, 1191

Uzdensky, D. A., 2002, ApJ, 574, 1011

Uzdensky, D. A. 2004, Ap&SS, 292, 573

Uzdensky, D. A. 2005, ApJ, 620, 889

van Putten, M. H. P. M. & Ostriker, E. C. 2001, ApJ, 552, L31

van Putten, M. H. P. M. & Levinson, A. 2003, ApJ, 584, 937

Vlahakis, N. & Königl, A. 2001, ApJ, 563, L129

Vlahakis, N., Peng, F., & Königl, A. 2003, ApJ, 594, L23

Woosley, S. E. 1993, ApJ, 405, 273

Yi, I. & Blackman, E. G. 1998, ApJ, 494, L163

Yoon, S.-C., & Langer, N. 2005, A&A, 443, 643

Zeh, A., Klose, S., & Hartmann, D. H. 2004, ApJ, 609, 952

Zhang, W., Woosley, S. E., & MacFadyen, A. I. 2003 ApJ, 586, 356